ANGULAR OPTICAL TRAPPING AND ITS APPLICATION TO DNA STRUCTURES

A Dissertation

Presented to the Faculty of the Graduate School

of Cornell University

In Partial Fulfillment of the Requirements for the Degree of

Doctor of Philosophy

by

Scott Forth

August, 2009

ANGULAR OPTICAL TRAPPING AND ITS APPLICATION TO DNA STRUCTURES

Scott Forth, Ph. D.

Cornell University 2009

DNA experiences constant mechanical stress in the cell, due to the action of enzymes and DNA-binding proteins. As a result, understanding the elastic properties and response to external stress is important in determining how DNA functions in vivo. Linear optical trapping has been employed previously to stretch DNA and measure its force-extension relationship. However, DNA is helical and is subject to winding, melting, and twisting during all parts of the cell cycle. Hence, measuring the response of DNA and DNA-based structures to torsional strain is equally (if not more) important. To this end, we have developed an angular optical trapping instrument which can detect and exert torque and twist, in addition to force and displacement. The torsional response of natural B-form DNA was studied, and an abrupt transition into a plectonemic state was observed for the first time. The Holliday junction, a four-way cruciform structure which is critical in DNA repair pathways, was also studied, and it was determined that this structure behaves like a nano-torque wrench, relieving torsional strain and promoting extensive branch migration events.

BIOGRAPHICAL SKETCH

Scott Thomas Forth was born to Thomas and Karen Forth on November 27th, 1978 in Mentor, OH. He moved with his family to Orchard Park, NY, just outside of Buffalo, NY shortly thereafter. While growing up in Orchard Park he attended Ellicott Elementary School, Orchard Park Middle School, and Orchard Park High School, from which he graduated as Salutatorian in 1997. He enrolled in Oberlin College and Conservatory's Double Degree program, simultaneously pursuing a degree in physics as well as musical performance, with percussion being his specialty. He spent several of his summers engaged with the Research Experience for Undergraduates (REU) programs at the University of Michigan, Cornell University, and the University of Pittsburgh. He completed an Honors project at Oberlin, studying the absorption of hydrogen in fullerene systems. It was these various experiences that led him to pursue further advanced study in the sciences. He graduated with highest honors in Physics, and both a Bachelors of Arts degree and Bachelor of Music degree in 2002, and subsequently enrolled in the graduate school at Cornell University. In 2004 he joined Michelle Wang's single molecule biophysics lab full time. Within the lab he has helped develop and employ an angular optical trapping instrument, with which he has studied the response of various DNA structures to external torsion. He graduated with a Masters of Science in 2007 and a Doctor of Philosophy in 2009, both in physics. In his spare time, he enjoys playing music, cooking, watching movies, spending time with friends, and traveling.

To my parents Thomas and Karen and my girlfriend Becky

ACKNOWLEDGMENTS

I would like to begin first and foremost by thanking my advisor, Michelle Wang, for the endless support she provided throughout my tenure in her lab. Her tireless dedication to research and her students is inspiring, and her willingness to teach in addition to motivate is a breath of fresh air. I admire her creativity and her drive to succeed, and have learned a great deal not only about the science itself, but about how to present and publish that work in a way that makes it compelling to others.

I am grateful to several other professors and committee members as well, notably Jim Sethna, Mukund Vengalattore, and Sol Gruner. They have provided excellent guidance, advice, collaboration, and intellectual stimulation. Jim Sethna in particular, with whom our group has worked closely, has been quite helpful in many theoretical aspects pertaining to the work in this dissertation. The collaboration between our experimental and theoretical groups has been enjoyable and fruitful.

There are many people from the Wang Lab who I would like to thank. First, I want to acknowledge Chris Deufel for his constant support and help throughout all aspects of my graduate career. His energy and drive are truly inspirational, and without his leadership, guidance, collaboration, and assistance, this certainly would have been a longer and more terrifying journey.

I would like to thank Maxim Sheinin and Arthur LaPorta, who both played a great role in assisting my understating of the angular trapping technique. Both have amazing theoretical and technical skills, and it has truly been a pleasure to have learned from them. Dan Johnson, Lucy Bai, Alla Shundrovsky, and Dave Wacker provided

incredible support in the wet-lab during my tenure. I really knew next to nothing about experimental biology coming in, and all of these former lab members patiently taught me what they knew, and helped me feel comfortable with the field. Michael Hall, Ben Smith, Jing Jin, James Inman, and Bert Fulbright all deserve thanks as well, for help with programming, biology, and instrument maintenance, as well as for wonderful conversation and friendship both in and out of the lab.

I would like to thank my undergraduate thesis advisor, Stephen FitzGerald, for his guidance and support during my honors project. It was in large part due to my enjoyment of that experience that I decided to attend graduate school in physics and pursue science as a career. I would also like to thank my percussion professor, Michael Rosen, who is truly one of the most fascinating and influential people I've met. His musical instruction was invaluable, and his passion for life (its finer elements and its simple pleasures) has been a source of motivation for a long time.

Finally, I would like to thank my wonderful family. My parents, Thomas and Karen Forth, have been endlessly supportive throughout my entire academic career. They encouraged my love of music, and were supportive when I decided to pursue a degree at the college level, and then again when I decided to pursue a Ph.D. in physics. They have always been there, and for that I am eternally grateful. Thanks go to my sister, Rebecca, who has always provided encouragement and inspiration. I'd like to acknowledge my grandparents for their incredible devotion to their families, as well as my aunts, uncles, and cousins. And, last but most, I'd like to extend a special thanks to my girlfriend Becky, whose love and support has helped me beyond words. You are absolutely the best, and I couldn't have done this without you. Your love means the world to me; thank you.

TABLE OF CONTENTS

LIST OF FIGURES

CHAPTER 1:

THE ANGULAR OPTICAL TRAPPING METHOD

TRADITIONAL OPTICAL TRAPPING TECHNIQUES

Optical trapping is a versatile technique with many applications in the field of single molecule biophysics. With its ability to measure minute forces (picoNewtons) and displacements (nanometers), it has proven to be a highly valuable tool in the study of molecular motors and biopolymers (Perkins, 2009). In this chapter, several salient features of the technology will be discussed, with the goal of providing enough information to satisfactorily understand the experiments performed throughout this work.

A conventional optical trap consists of a single Gaussian TEM_{00} mode near-infrared laser, with a typical wavelength of 1064 nm, focused to a diffraction limited spot with a high NA (> 1.3) microscope objective (Ashkin et al., 1987). A dielectric particle found very near the focus will experience a force which can be decomposed into two parts; a scattering component and gradient force component (Svoboda and Block, 1994). The scattering force may simply be thought of as the transfer of linear momentum from the photons of the laser beam traveling along the axial direction to the particle, resulting in the particle being pushed downstream (as would be experienced by a ball in a stream of water from a hose, for example). The second component, the gradient force, results from the fact that the dipole induced in the dielectric particle as a result of being placed in an oscillating electric field (whose frequency is lower than the resonance of the dipole) will be drawn towards the region of highest intensity, i.e., the laser focus. Thus, the main requirement for producing a stable trapping beam is an extremely sharp intensity gradient, a condition made possible by using an objective of high numerical aperture. In the Raleigh limit

(particle radius << wavelength of laser light), the gradient component of the trapping force may be written as:

$$F_{grad} = \frac{2\pi a^3}{c}\left(\frac{m^2 - 1}{m^2 + 2}\right)\nabla I$$

$$F_{grad} \propto \nabla I$$

where a is the radius of the trapped particle, m is the ratio of the index of refraction of the particle to the surrounding medium, and I is the intensity of the laser light (Neuman and Block, 2004). Thus, the three dimensional restoring force is simply proportional to the intensity gradient, which, when properly designed, is extremely steep in all three spatial dimensions. Most tweezers monitor forces and displacements in the lateral dimensions. Recently it has been shown that quantitative measurements can be made with high accuracy in the axial dimension as well (Deufel and Wang, 2006).

In order to make high-precision quantitative measurements of forces and displacements exerted on biological molecules, a careful position and force calibration must be performed. Typically, this is done by monitoring the position and divergence of the outgoing beam, after the beam has interacted with the trapping particle, with a position sensitive photo-detector, such as a quadrant photodiode. Any deviation in the light's position is related to the change in linear momentum of the beam, or the force exerted on the beam by the trapped particle. By fixing the bead to a surface which is mounted on a high precision piezoelectric stage and displacing it by a known amount, the conversion from detector voltage to real units of distance can be known. Monitoring the Brownian fluctuations of the trapped bead and applying the

equipartition theorem for an object trapped in a harmonic potential will yield information about the trap stiffness; specifically:

$$\frac{1}{2}k_B T = \frac{1}{2}k_x \left\langle x^2 \right\rangle$$

where k_x is the trap stiffness in a particular dimension of the trap. This relation holds for the lateral dimensions as well.

Figure 1.1 schematically depicts a very basic optical trapping setup. It is advantageous to design such a trapping setup around an inverted microscope, as visualization of the specimens to be optically manipulated can be quite useful. Additionally, many commercially available microscopes come equipped with optics and filters for fluorescence imaging, a visualization technique which can be integrated into an optical tweezers instrument. It is possible to design an optical trap using a dual objective configuration, removing the optics from the confines of the microscope, and is desirable if either space or mechanical stability of the components are crucial issues.

Of the many design considerations, the careful mapping of optically conjugate planes is primary. With proper mapping, the laser trap in the specimen plane can be steered at multiple locations (such as a beam steering AOM, a translating telescope lens, or a micromechanical mirror) with minimal aberrations to the trap. Additionally, the beam entering the back focal plane of the objective must be expanded so as to overfill this plane, often by a radial factor of 1.2 to 1.4. This ensures that the high angle rays which have entered the objective near its aperture edge have adequate intensity to provide effective trapping.

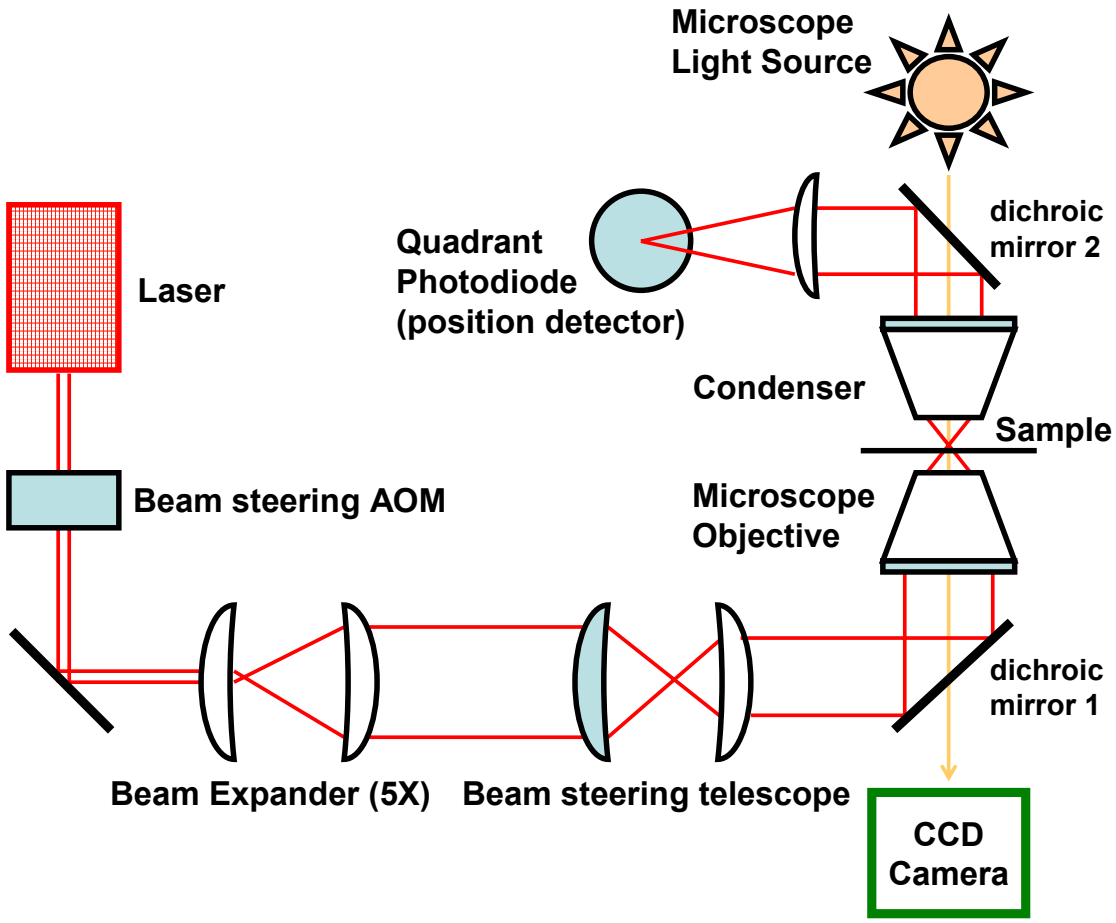

Figure 1.1: A schematic of a generic optical trap. The trapping laser is expanded so as to overfill the objective back aperture. After interacting with the sample, the light is collected and its position is recorded, which gives information about the change in momentum (d*p*/dt = force) and location (position) of the beam at the sample. All optics shaded with light blue are in optically conjugate planes. Of primary interest are the Beam Steering AOM and the Beam steering telescope, both of which function to laterally displace the trap in the specimen plane without changing its shape and therefore trapping properties.

With a conventional optical trap, measurements of extension and force applied can be measured. For instance, the amount of force it takes to disrupt individual nucleosomes assembled on a long DNA segment has been reported (Brower-Toland et al., 2002). The procession of an RNA Polymerase molecule along its DNA substrate has been directly monitored as it undergoes transcript elongation (Adelman et al., 2002), and the pausing kinetics of the molecule have been studied (Bai et al., 2004). The powerful technique of DNA unzipping allows for the measurement of a protein's binding location to better than 2 base pairs (Hall et al., 2009; Johnson et al., 2007). In this technique, the two strands of the DNA duplex are mechanically separated with force applied by the optical trap. The DNA is sequentially unwound at a fixed rate. If a protein is bound to the DNA, the force required to disrupt the interaction increases, giving rise to a very strong force signal peak (Koch et al., 2002). As an example, Figure 1.2 shows the unzipping of a template which contains the estrogen receptor element (ERE), located 127 base pairs downstream of the initial unzipped base. In the presence of estrogen receptor protein, a well studied transcription factor, the force rises sharply at this location, indicating a relatively strong binding affinity to that particular sequence. While the location of this particular protein-DNA interaction is well known, there are countless proteins which interact with DNA whose sequence dependence and binding affinities are not well characterized; the unzipping technique provides a powerful tool by which to study such interactions.

While the traditional optical tweezers method has been proven to be powerful and useful, it can only provide measurements of force and displacement. Many biological processes, especially those involving DNA (whose structure is famously known to be helical) must exert or be regulated by torque, and must involve significant angular motion as well.

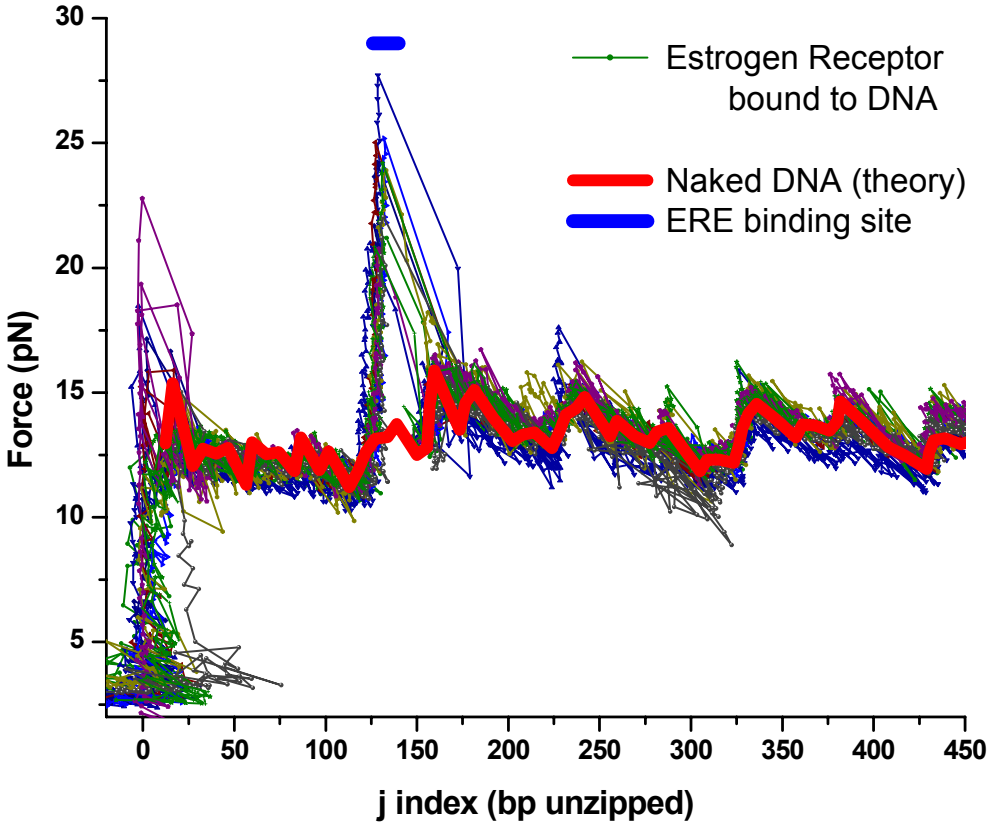

Figure 1.2: An example of data taken using a traditional linear optical trap. The two stranded of duplex DNA are mechanically unzipped starting at a particular location along the DNA template (base 0). Unzipping proceeds along the template, with a force baseline on the order of 12-15 pN. There is noticeable sequence dependence in the naked DNA force signature, owing to the fact that G-C base interaction, with 3 hydrogen bonds, requires a great force to disrupt than do A-T base pairs, with only 2 hydrogen bonds. In this example, a protein, the estrogen receptor, is bound at a particular strong binding sequence, located at bases 127-139. Once the unzipping fork has encountered this interaction, the force increases far above baseline, as additional force is needed to pop the protein off the template. In this manner, identification of protein binding locations and affinities may be studied.

THE NEED FOR ANGULAR INFORMATION

While it is the case that a conventional optical tweezers instrument applied to a biological system can provide a myriad of information, it certainly cannot provide knowledge about the totality of an enzyme's mechanical action. That is to say, an OT can provide accurate measure of forces and displacements, but cannot speak to the torques or angular displacements; for example, many enzymes which act on DNA (such as RNA polymerase or topoisomerases) certainly pull on their substrate as they translocate, but, due to DNA's helical structure, they must also twist and apply torque to the DNA in the process (Harada et al., 2001). To this end, our lab has developed an angular optical trapping instrument, capable of simultaneous measurement of force, position, torque, and angular displacement (La Porta and Wang, 2004), in addition to developing birefringent trapping particles with specific biological functionalization for use in DNA-based single molecule assays (Deufel et al., 2007).

The angular optical trap works by the principle that an optically anisotropic particle (and, in our particular case, a uniaxial birefringent cylinder) will be in its stable trapping configuration if the extraordinary crystal axis (which is more easily polarized than the other two ordinary axes) is aligned with the incident electric field (Bishop et al., 2003; Nieminen et al., 2001). As the electric field is rotated, the particle will respond by tracking the field and hence itself rotate. If there is a misalignment between the E-field of the trapping laser and the induced polarization in the particle, a restoring torque will be exerted by the light in an attempt to return the particle to its stable state (Figure 1.3).

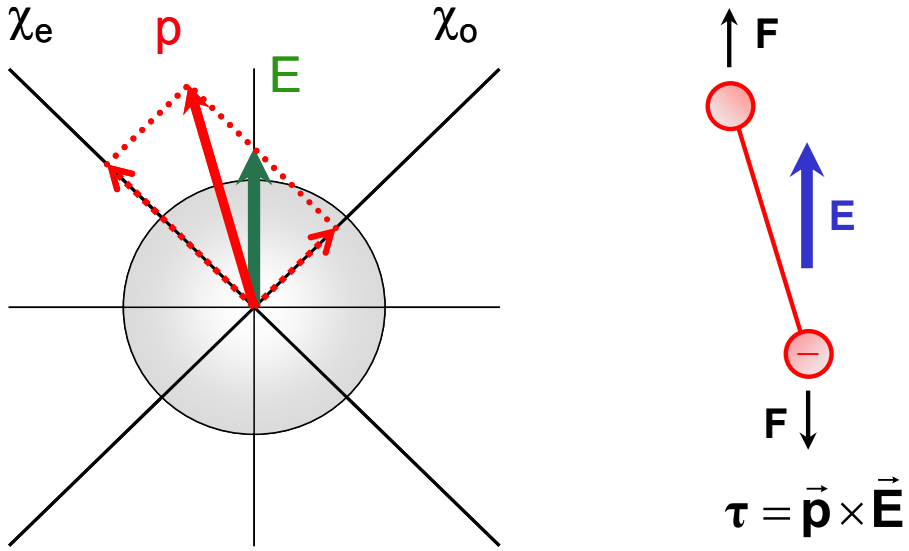

Figure 1.3: Left: An optically anisotropic particle with positive uniaxial birefringence will be more easily polarized along one axis (χ_e) than the other two (χ_0). Right: If there is a misalignment between the applied electric field and the induced polarization vector, a restoring torque will attempt to realign the two and return the particle to its state of minimum energy.

METHOD FOR GENERATING ROTATING LINEAR POLARIZATION

In order to have full control over the angular orientation of the particle, it is necessary to be able to generate a linear polarization state in the trapping plane with arbitrary angular orientation, and to be able to update the polarization state at better than kilohertz rates. Several possible methods for control of polarization rotation exist, including mechanical rotation of an optical component, such as a half-lambda plate, or an electro-optic modulator (EOM), but both methods have significant shortcomings such as speed, mechanical stability, and rotation range. In particular, the EOM is capable of introducing a precise phase shift between orthogonal components up to 2π radians. Upon reaching this maximum limit, for smooth rotation of the output polarization to be achieved, the phase shift must immediately be reset to 0 radians. This process involves a voltage jump across the EOM crystal on the order of tens of kiloVolts, which can be slowed significantly if extreme care is not taken in the design of the control circuitry. In addition, the EOM method allows only for the generation of purely linear polarized trapping beams. There are instances where circularly polarized traps could be useful, such as exerting a fixed torque on the trapped particle, or superimposing two incoherent circular beams to generate a zero torque trapping state.

To overcome these design limitations, we have employed a pair of acousto-optic modulators (AOM) which allows for nearly instantaneous setting of the polarization angle, and a very simple and elegant method for generating rapid and smooth rotation rates well into the tens of kilohertz regime.

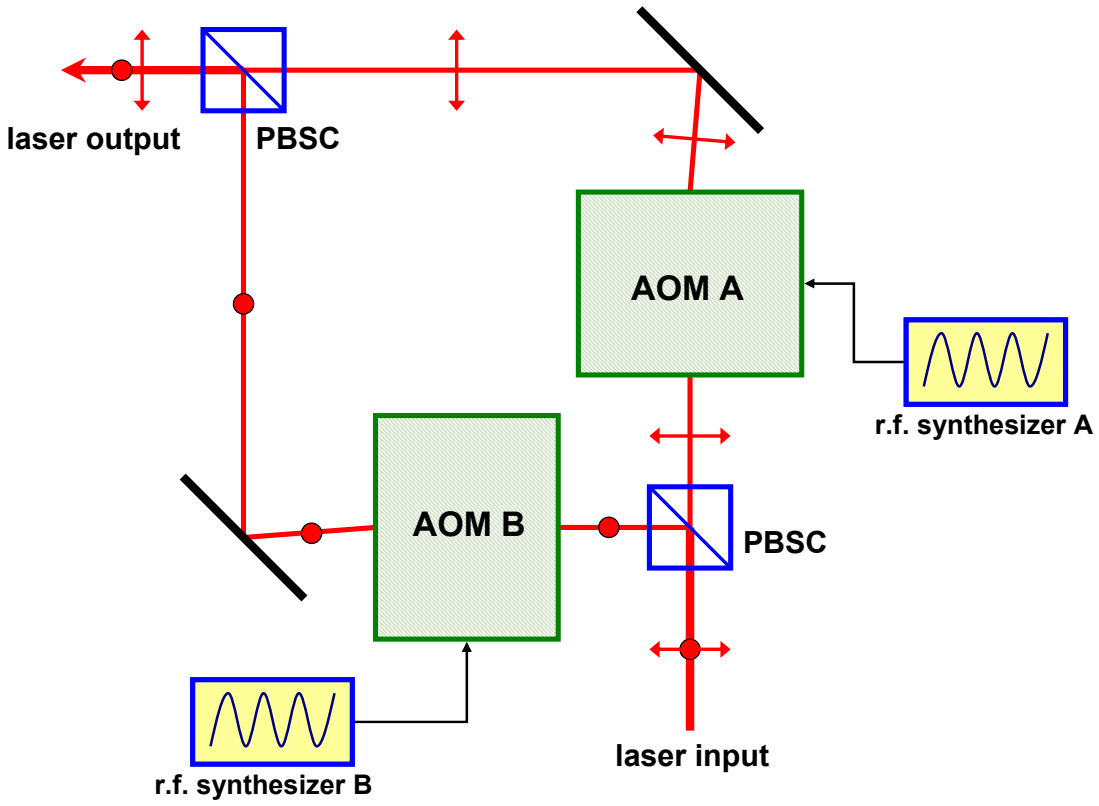

Figure 1.4: Generating an arbitrary polarization state using two AOMs. A linearly polarized *laser input* is rotated by 45º relative to the S and P polarization directions, which correspond to out of the page and parallel to the page, respectively. A polarizing beam splitting cube (*PBSC*) splits the two components accordingly, after which each beam passes through an acousto-optic modulator (*AOM*). Each AOM is driven by a unique computer controlled r.f. synthesizer. The deflected beams are frequency upshifted by ~40 MHz, and are subsequently recombined at a second *PBSC*. The *laser output* then consists of a single beam with equal amplitudes of S and P polarization, but with an arbitrary relative phase shift of φ between them.

Prior to the AOMs, the laser beam is linearly polarized and rotated at an angle of 45º relative to the subsequent optics, as shown in Figure 1.4. The beam then interacts with a polarizing beam splitting cube, which passes a "P" polarized beam and reflected an "S" polarized beam, each with equal intensity. The two beams then each are deflected by their respective AOM. A dual channel computer-controlled digital frequency synthesizer generates an r.f. (radio frequency) sine wave with center frequency near 40 MHz, which is amplified to a power up to 5 W and sent to the input of each AOM. The first order diffracted beam intensity is controlled by the magnitude of the r.f. wave, which can be easily and rapidly controlled via computer. The interaction of the light wave with the traveling soundwave results in a frequency upshift of ~ 40 MHz in the diffracted beams, as result of the photon-phonon interaction intrinsic to the operation of the modulators. The two orthogonally polarized beams are then brought together at a second polarizing beam splitting cube and recombined at the output. At this point, the relative phase of the wavefronts is arbitrarily shifted by some phase φ, and the polarization state immediately after recombination is arbitrarily elliptically polarized. It should be noted that utmost care must be taken to ensure that the beams exiting the recombination cube are perfect collinear, a process which requires meticulous alignment of both mirrors and the cube itself. If the beams do not exit the rotation apparatus collinearly, several problems may emerge, including trap anisotropy, suboptimal rotation, and significant imperfections in the detection signals.

After the recombination of the beams, the light travels a distance through minimal beam expansion optics and a series of mirrors to bring it into the back focal plane of the microscope objective. The beam traveling this optical path has equal intensities of "S" and "P" polarized light, but with a phase shift between the components introduced by the AOMs. Just prior to the objective, a quarter lambda plate is mounted, rotated

by 45º relative to the S and P polarization directions. After passing through the λ/4 plate, a phase shift is introduced to each of the components, the result of which is a linearly polarized state rotated by an angle θ. This transform of an elliptically polarized state to a rotated linear state is depicted in Figure 1.5. In the case where the phase shift between the S and P components is 0, the state is already linear; it is transmitted along the slow axis of the λ/4 plate and no phase shift is applied; the beam emerges linearly polarized at the same angle it entered (for ease of discussion, the angle θ can be defined according to the figure as 45º relative to the vertical). In the case where the phase shift between the S and P components is 90º, the state may be described as circular; after it interacts with the λ/4 plate, it has been converted to a linear state with θ = 90º. Phase shifts between these two cases will result in an incoming beam which is elliptically polarized and an output beam which is linearly polarized. Note that due to the degeneracy in the electric field direction (an electric field oriented along 0º is indistinguishable from a field oriented along 180º), the change in polarization angle θ is half the magnitude of the phase differential between the AOMs, Δφ; that is to say, $\theta = \Delta\varphi/2$.

As an illustrative example, imagine we wish to rotate a particular in the sample plane at a rate of one turn per second. This is easily accomplished by driving the two AOMs with r.f. signals which differ in frequency by 2 Hz (for instance, AOM A is driven at 40 MHz and AOM B is driven at 40.0000002 MHz). The result after the beams are recombined will be a smoothly time varying phase shift φ(t) between the two orthogonal components. After transformation by the quarter lambda plate, a rotation linear state is generate in the sample plane, with angular frequency $\omega = \frac{1}{2}\, d\varphi/dt = 1$ Hz.

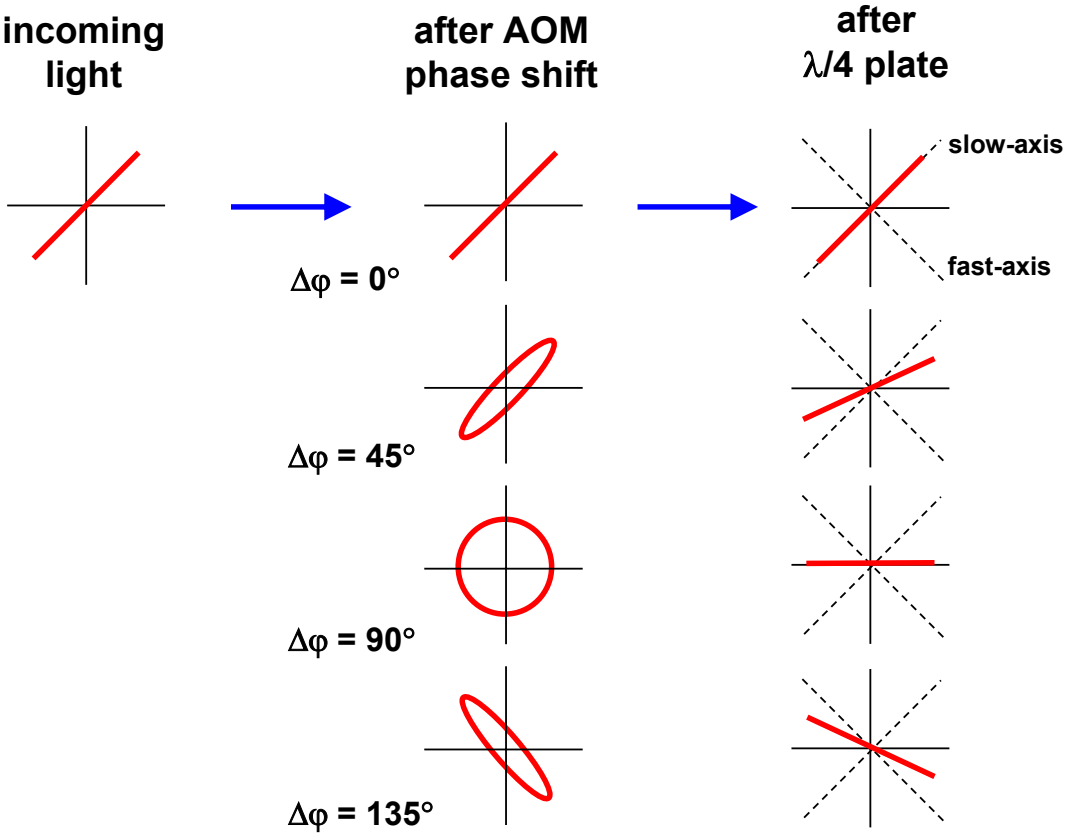

Figure 1.5: Converting an arbitrary elliptical polarization state into a rotated linear state using a quarter wave plate. The laser light entering the rotation apparatus is linearly polarized, and therefore consists of equal amplitudes of S and P polarization which are completely in phase. After interacting with their respective AOMs, a relative phase shift between the components is introduced, resulting in an arbitrary elliptical state. The beam then passes through a quartz wave plate, which shifts the polarizations along its slow and fast axis by 90º. For each polarization state, the effects of the quarter wave plate are shown, with the resulting output being a linearly polarized beam rotated by angle θ, where θ = Δφ/2.

DETECTION OF THE POLARIZATION STATE

In order to acquire precise angular position data, the polarization state of the trapping beam must be known; specifically the angle of the linearly polarized state relative to the sample plane and the residual ellipticity in the beam. To accomplish this, an angle detection scheme has been implemented, allowing accurate measurement of those two important parameters.

After the beam is recombined (the final stage in the rotation apparatus), it is directed through a Beam Tap (Spiricon, Inc.), which samples a small fraction of the light (less than 1%), while passing the majority (greater than 99%) for use in the trap itself. During typical optical trapping experiments, between 50 and 500 mW of light enter the microscope objective, while between 0.5 and 5 mW are sampled for angle detection. The input detection scheme is divided into two measurement components, the ellipticity detector, which monitors the relative intensity of the S and P light components, and the angle detector.

The major features of the input detection apparatus are depicted in Figure 1.6. The small fraction of sampled light is split into nominally equal components by a 50/50 non-polarizing beam splitting cube. The reflected path travels to a PBSC, which reflects the S and transmits the P component. The beams are impingent upon two silicon photo-detectors (UDT Electronics), each of which has its own on-board op-amp for signal amplification. These detectors accurately reflect the amount of S and P light in the beam; careful calibration is done by comparing the voltage outputs of the detectors with that of a power meter placed upstream directly after the AOMs. An

appropriate gain is applied in software such that the power in each beam path can be easily converted into the real world units of mW.

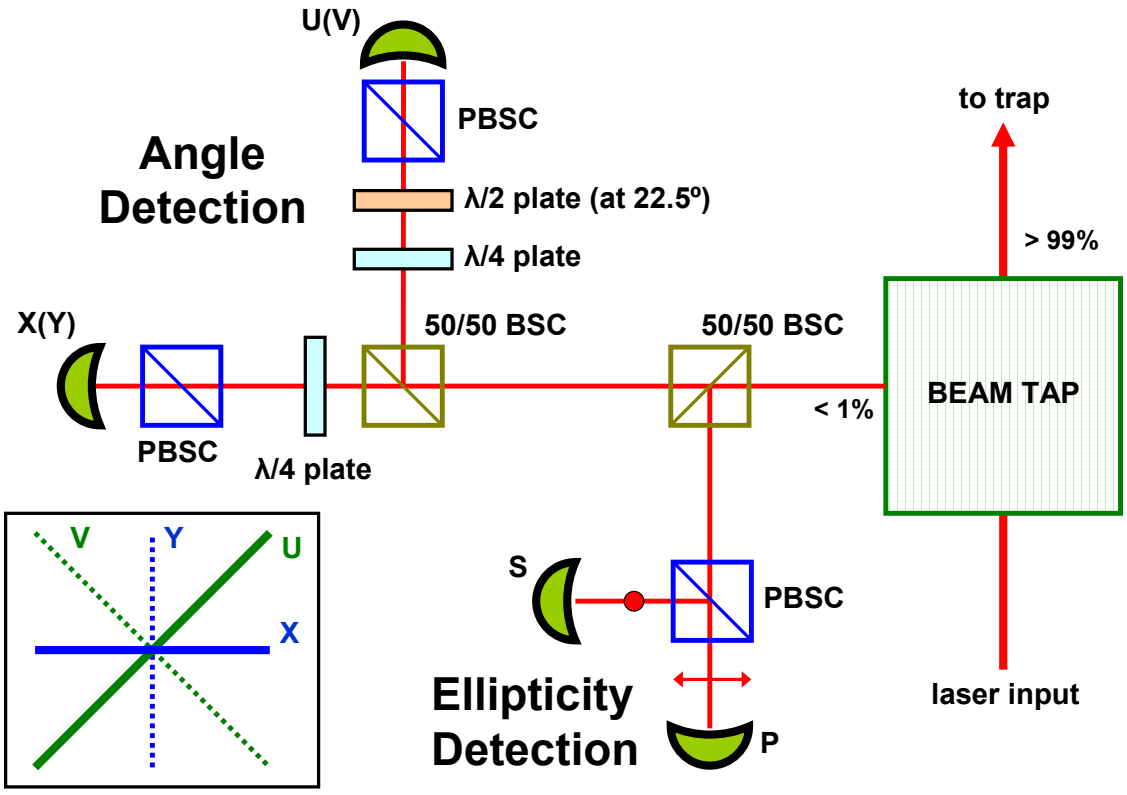

Figure 1.6: The angle detection scheme. Both the input ellipticity and angular orientation of the trapping beam are monitored upstream of the trap. Inset at lower left describes the polarization components as measured by the Angle Detection component of the system. X and U are measured directly by the photo-detectors, while Y and V are inferred from the measured values.

The input angle detection is accomplished by splitting the beam into two paths, each of which contains a quarter lambda plate to transform the light into the same linear rotating state that will exist downstream in the sample plane. In order to successfully determine the angular orientation for all possible values, it is necessary to use multiple detectors; one to monitor the component in the X (horizontal direction), and one to monitor the U (45º relative to the horizontal) component. Because of the symmetry of the system, we can infer the magnitudes of the orthogonal components (Y and V respectively) by tuning the input angle detector gains such that the maximum intensity achievable is equal to the sum of the S and P ellipticity detectors. That is to say, $Y = (S + P) - X$ and $V = (S + P) - U$. We can therefore determine the magnitude of the electric field in each quadrant, and derive the field orientation θ with the following relation:

$$\tan(2\theta) = \left(\frac{(Y - X)(U + V)}{(U - V)(Y + X)} \right).$$

Figure 1.7 shows simulated detector signals and the corresponding calculated polarization angle across the full range of possible AOM phase shifts. Note that the angle theta can be measured modulus π only due to the symmetry of the electric field (oscillations along the polarization angles 0 and π, for instance, are equivalent, and are therefore indistinguishable in any detection apparatus). Measuring angles greater than π is easy achieved, however, by carefully employing software to perform a rollover calculation when the angle crosses π radians.

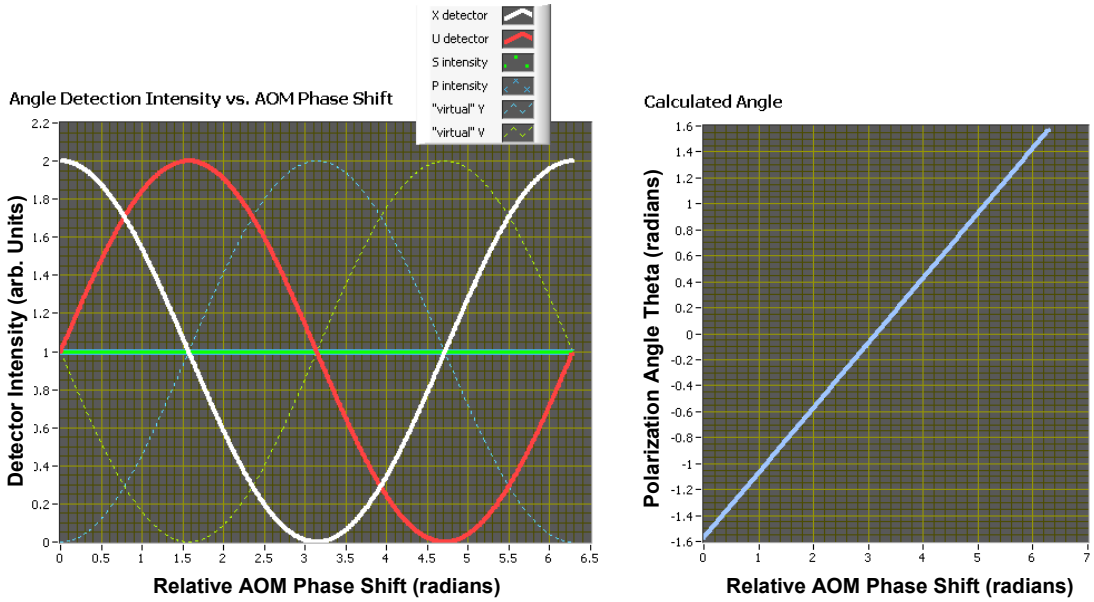

Figure 1.7: Input detector signals as the AOM phase is varied. The left panel depicts detector voltages as measured with the four input detectors. The S and P intensity (green and blue) are independent of the relative AOM phase shift, as expected. The X and U intensities (white and red) show an oscillatory pattern, as the linearly polarized light rotates and is passed through a polarization analyzer. Because of the system symmetry, the Y and V components of the polarization may be inferred from the measured X and U (dashed aqua and yellow), reducing the required number of detectors. At right is the relation between the calculated angle θ and the relative phase shift introduced by the AOM rotator.

DETECTION OF TORQUE

Just as force detection is performed by monitoring the change in the trapping beam's linear momentum, torque detection here may be accomplished by measuring the change in angular momentum of the trapping beam. Light entering the trap is linear (or, equivalently, contains equal amounts of left- and right-handed circularly polarized light), and hence, has no net spin angular momentum. If it exerts a torque on the particle, the output light becomes elliptically polarized, and hence is composed of ***unequal*** amounts of left- and right-handed polarized light. By measuring the relative power of the L and R components of the output beam as shown in Figure 1.8, we, in theory, have a direct measurement of the torque exerted on the particle/biological molecule (Bishop et al., 2004). In practice, because it is impossible to collect 100% of the outgoing light, we must calibrate the differential power signals to achieve an accurate measurement of torque in physical units.

In addition to the torque detector, our instrument has a quadrant photodiode detecting the position of the output beam as well, just as in standard linear optical trapping. However, due to the shape anisotropy of our cylindrical trapping particles, a calibration of detector signals is challenging, as lateral translation in the trap is difficult to distinguish from particle tilting, an effect which arises when tension is applied unevenly to the trapped probe. Thus, the quadrant photodiode is used for a qualitative measurement of the centering of the DNA tether relative to the trap, but accurate and precise quantitative information is unattainable.

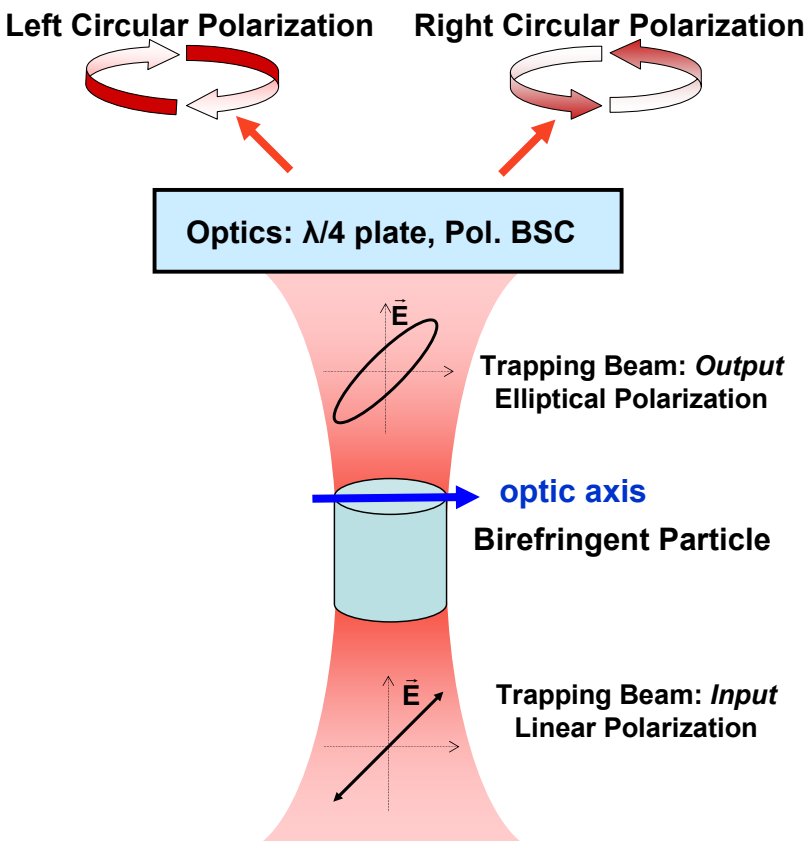

Figure 1.8: Schematic of the torque detection scheme. Light entering the trap is linearly polarized with the E-field's angular orientation, and has zero net angular momentum. After interacting with a trapped particle, the light may become elliptically polarized, resulting in a change in angular momentum (d*L*/dt = torque) which may be measured as an imbalance in the power of right circular versus left circular components of the transmitted beam. This accomplished with a quarter wave plate aligned with the same orientation as the previous waveplate, and serves to map the linear state back into its S and P components. A PBSC divides the polarizations, which subsequently impinge on photo-detectors to measure the intensity of each component. The difference in the intensity signals corresponds to the angular momentum change, and hence the torque, in the beam.

NANOFABRICATED QUARTZ CYLINDERS AS BIOLOGICAL HANDLES

In order to acquire highly precise and reproducible single molecule measurements, handles must be employed in order to couple the DNA molecule of interest to the optical trap. In conventional optical trapping setups, commercially available polystyrene beads with radii on the order of several hundred nanometers to one micron are often used. These particles are almost perfectly spherical and can easily be filtered by size to ensure that a given batch is uniform to within a few percent. This greatly facilitates the calibration process, as particle to particle variation is minimal. Additionally, these particles can easily be surface functionalized with specific proteins, such as streptavidin, for attachment to biological substrates, like biotinylated DNA.

In the case of the angular trap, however, no such off-the-shelf products are available. Thus, suitable particles for angular trapping needed to be designed and manufactured within our own lab. To this end, birefringent nanofabricated cylindrical particles were designed and fabricated at the Cornell NanoScale Science and Technology Facility (CNF) to be employed as handles for torsional manipulation of DNA and facilitate calibration, precision, and measurement reproducibility (Deufel et al., 2007). The cylinders, made from optically birefringent quartz, are highly uniform, and due to their aspect ratio, orient in the proper vertical orientation in angular trap (that is, with their long axis along the laser's propagation direction). The extraordinary axis of the material was selected to be in the radial direction of the cylinder; thus, rotation is applied along the long axis of the particle. The cylinders are biologically functionalized on a single end for specific attachment to a multiply biotinylated DNA molecule (Kleinfeld et al., 1988). One single "x-cut" four-inch wafer of crystalline

quartz yields approximately two billion cylinders of height one micron and diameter 500 nm (Figure 1.9), enough for over a thousand single molecule experiments.

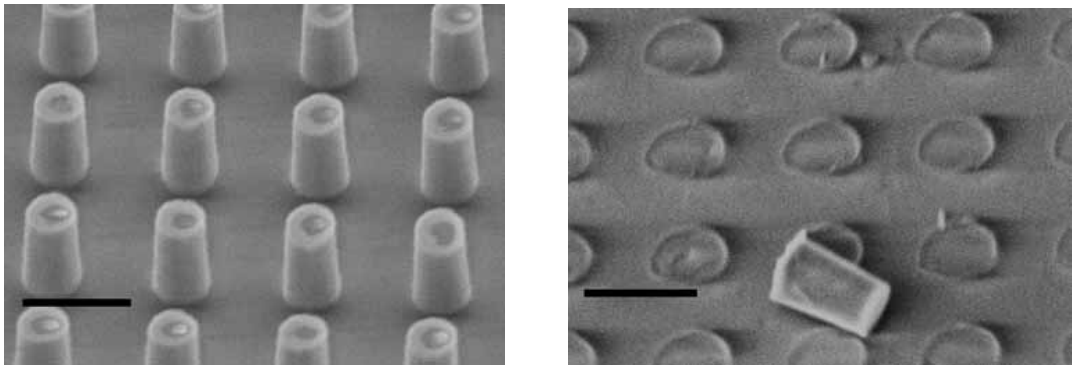

Figure 1.9: Left: SEM image of a small segment of nanofabricated quartz pillars. The pillar diameter is ~500 nm, while the height is ~ 1 micron. The top surface is specifically functionalized with 3-aminopropyltriethyoxysline to which Streptavidin protein can be cross-linked for subsequent attachment to biotinylated DNA. Right: After mechanical cleavage, a single quartz cylinder remains. The majority of these cleaved cylinders are collected and suspended in solution for use in angular optical trapping experiments.

CALIBRATION METHODS

To obtain accurate measurements with physical units, a calibration must be performed which allows the optical intensities (read from the output photo-detectors as a voltage) to be converted to radians (angle) or pN-nm (torque). There are therefore two primary calibration relationships which must be determined: the angular sensitivity, or voltage change per angular deviation from the input polarization; and angular trap stiffness, which is the amount of torque exerted per radian, analogous to the classical Hookeian spring constant, k.

The angular sensitivity is determined by first trapping a free cylinder. The polarization is then rotated at a rate much faster than the particle can track; at low powers (less than 50 mW), a rate of 400 Hz is sufficient. As the polarization rapidly scans the quasi-stationary particle, the signal from the torque detector is monitored. When the polarization is aligned with the extraordinary axis of the particle, the detector registers 0 V, as the torque experienced by the particle is zero. When the polarization vector is oriented 45º relative to the particle's extraordinary axis, the torque experienced by the particle is at its maximum, and the corresponding detector voltage reads its maximum value, V_0. As shown in Figure 1.10, the torque signal is nearly sinusoidal. The angular deviation, then, can be written as $\theta = \frac{1}{2}\sin^{-1}\left(\frac{V}{V_0}\right)$,

where V is the measured voltage at a given time. In the limit of small angular deviations between the particle's axis and the linear polarization, this can be expressed as $\theta = V / 2V_0$.

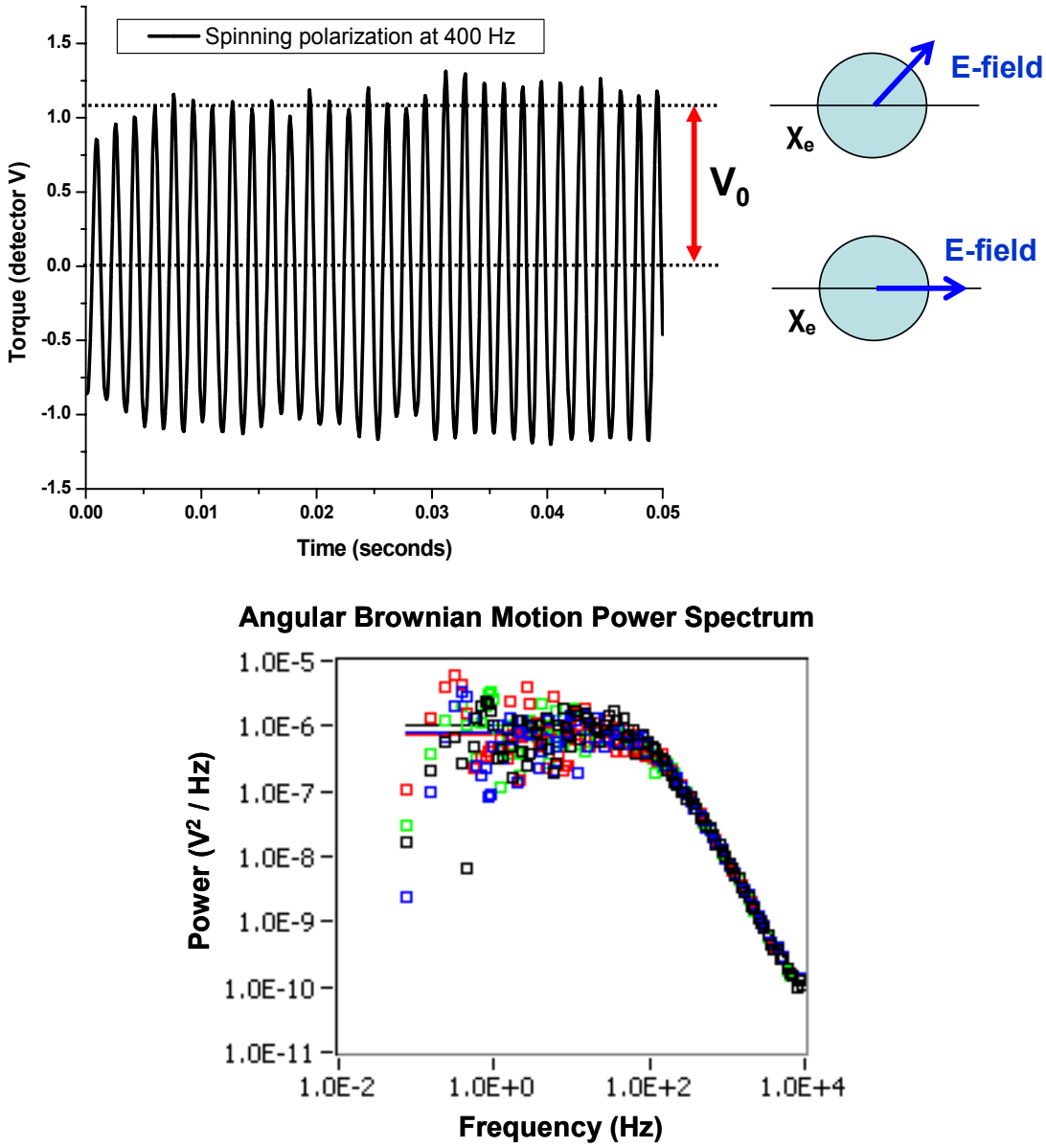

Figure 1.10: Calibration techniques. Top: A free cylinder is trapped, and the polarization is rotated much faster than the particle can track. The quasi-stationary particle is thus scanned by the laser polarization, and the maximum angular deviation can be correlated to the detector signal. Bottom: The power spectrum of a trapped cylinder. The power spectrum is directly related to the stiffness of the trap, and parameters such as the corner frequency and angular variance can be extracted from this data (Svoboda and Block, 1994).

The angular trap stiffness can be determined by trapping a free cylinder and monitoring the Brownian fluctuations, analogous to the method used to calibrate standard optical traps (Neuman and Block, 2004). For a particle trapped in a harmonic potential undergoing thermal Brownian fluctuation, the relation between the trap stiffness k_θ and the thermal energy can be given by $\frac{1}{2}k_B T = \frac{1}{2}k_{\boldsymbol{\theta}}\left\langle \boldsymbol{\theta}^2 \right\rangle$, where $\left\langle \boldsymbol{\theta}^2 \right\rangle$ represents the angular variance of the particle. In practice, the most effective way to measure the trap stiffness is to monitor the fluctuations of the particle for a short period of time (5 seconds is generally sufficient). It is important to acquire data at a sampling rate well above the corner frequency of the system. Typical corner frequencies for the angular trap are between 75 and 200 Hz, so a sampling rate of 5 to 10 kHz is often chosen.

The power spectrum of the acquired data is then taken, as shown in Figure 1.10 (bottom panel). Note that the conversion between detector voltage and angle must be known to obtain usable data, thus the angular sensitivity of the trap must first be determined. The power spectrum of an optical trapped particle is fit to a Lorentzian equation of the form $P(f) = \frac{A^2}{(f^2 + f_0^{\,2})}$, from which the amplitude A and corner frequency f_0 may be extracted. Knowing these two parameters, the area under the curve, which is the measure of angular variance, can be determined using the close form expression $\int_0^\infty \frac{A^2}{\left(f^2 + f_0^{\,2}\right)} df = \frac{\pi A^2}{2 f_0}$. The particle's angular variance may be computed from the measured time course of the particle directly, but due to intrinsic filtering effects in the system and a finite sampling bandwidth, this method loses high frequency information, and thus leads to an underestimation bias. Fitting the power spectrum does not suffer from this limitation, and is thus preferred.

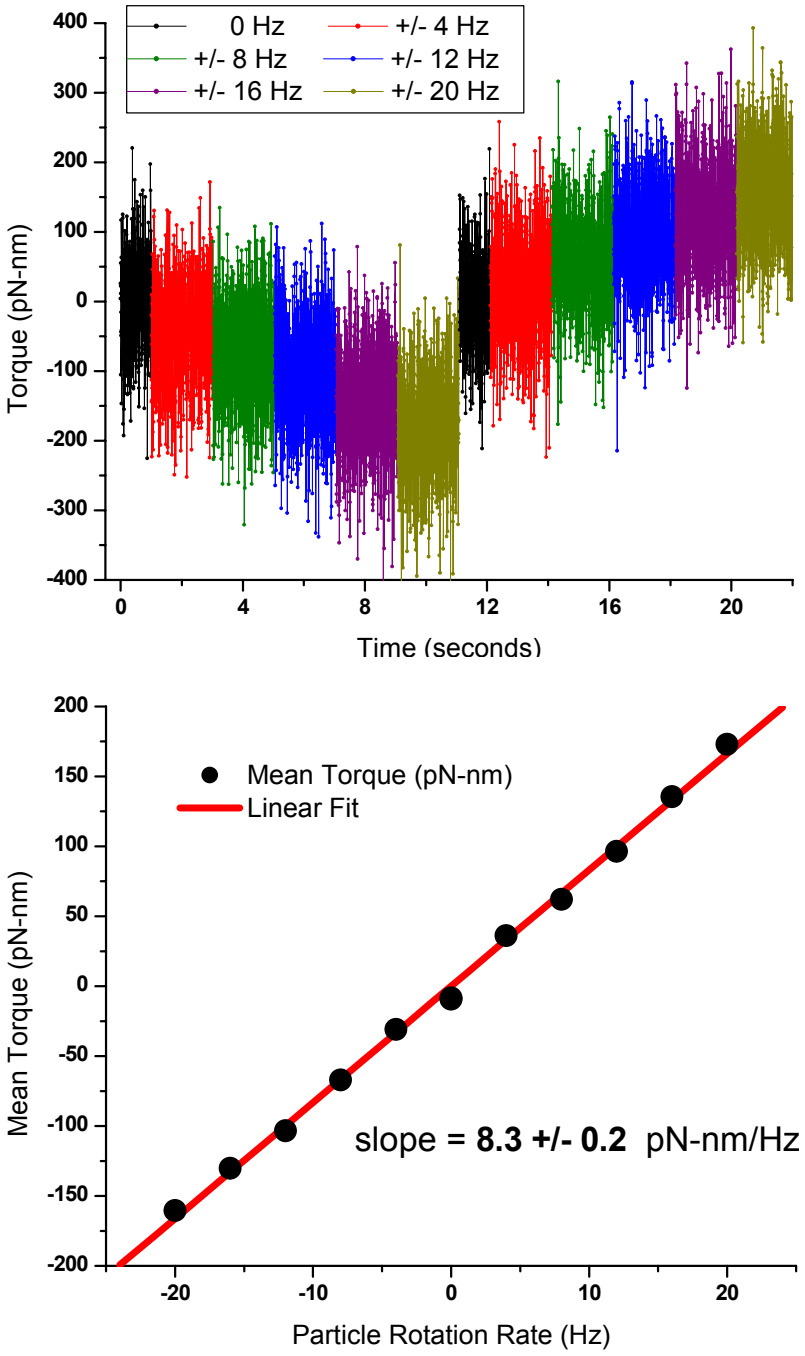

Figure 1.11: Measure of the viscous drag on a quartz cylinder. Top: The cylinder is rotated at various rates for a brief duration. The raw torque signal is shown versus time. Bottom: The mean torque value as a function of rotation rate. The relationship is linear, with the viscous drag coefficient as the slope.

FREE CYLINDER ROTATION

As a confirmation of the system's calibration, simple experiments involving free cylinders alone may be performed. As an example, a single free particle is trapped and rotated at various increasing rates, in both the positive and negative direction. The Stokes' viscous drag torque on a rotating sphere of diameter D depends linearly on the rate of rotation ω, as $\tau = \pi\eta D^3\omega$, where η is the viscosity of the fluid medium (La Porta and Wang, 2004). Experiments performed in our lab have shown that approximating the quartz cylinder as spherical is sufficient if the particle is located more than one radius away from the cover slip surface.

From the data in Figure 1.11, we find a viscous drag coefficient of 8.3 +/- 0.2 pN-nm/Hz, which yields a spherical particle radius of 380 nm, in excellent agreement with the known cylinder geometry. Thus, we are reassured that the system is well calibrated, and experiments involving biological substrates may be performed. Subsequent chapters will detail two such experiments: measurement of the torsional response of B-form DNA (Forth et al., 2008) and a careful study of the mechanical properties of the Holliday junction four way DNA structure.

REFERENCES

Adelman, K., La Porta, A., Santangelo, T.J., Lis, J.T., Roberts, J.W., and Wang, M.D. (2002). Single molecule analysis of RNA polymerase elongation reveals uniform kinetic behavior. Proc Natl Acad Sci U S A *99*, 13538-13543.

Ashkin, A., Dziedzic, J.M., and Yamane, T. (1987). Optical Trapping and Manipulation of Single Cells Using Infrared-Laser Beams. Nature *330*, 769-771.

Bai, L., Shundrovsky, A., and Wang, M.D. (2004). Sequence-dependent kinetic model for transcription elongation by RNA polymerase. J Mol Biol *344*, 335-349.

Bishop, A.I., Nieminen, T.A., Heckenberg, N.R., and Rubinsztein-Dunlop, H. (2003). Optical application and measurement of torque on microparticles of isotropic nonabsorbing material. Phys Rev A *68*, 033802.

Bishop, A.I., Nieminen, T.A., Heckenberg, N.R., and Rubinsztein-Dunlop, H. (2004). Optical microrheology using rotating laser-trapped particles. Physical Review Letters *92*, 198104.

Brower-Toland, B.D., Smith, C.L., Yeh, R.C., Lis, J.T., Peterson, C.L., and Wang, M.D. (2002). Mechanical disruption of individual nucleosomes reveals a reversible multistage release of DNA. Proc Natl Acad Sci U S A *99*, 1960-1965.

Deufel, C., Forth, S., Simmons, C.R., Dejgosha, S., and Wang, M.D. (2007). Nanofabricated quartz cylinders for angular trapping: DNA supercoiling torque detection. Nat Methods *4*, 223-225.

Deufel, C., and Wang, M.D. (2006). Detection of forces and displacements along the axial direction in an optical trap. Biophysical Journal *90*, 657-667.

Forth, S., Deufel, C., Sheinin, M.Y., Daniels, B., Sethna, J.P., and Wang, M.D. (2008). Abrupt buckling transition observed during the plectoneme formation of individual DNA molecules. Physical Review Letters *100*, 148301.

Hall, M.A., Shundrovsky, A., Bai, L., Fulbright, R.M., Lis, J.T., and Wang, M.D. (2009). High-resolution dynamic mapping of histone-DNA interactions in a nucleosome. Nat Struct Mol Biol *16*, 124-129.

Harada, Y., Ohara, O., Takatsuki, A., Itoh, H., Shimamoto, N., and Kinosita, K. (2001). Direct observation of DNA rotation during transcription by Escherichia coli RNA polymerase. Nature *409*, 113-115.

Johnson, D.S., Bai, L., Smith, B.Y., Patel, S.S., and Wang, M.D. (2007). Single-molecule studies reveal dynamics of DNA unwinding by the ring-shaped T7 helicase. Cell *129*, 1299-1309.

Kleinfeld, D., Kahler, K.H., and Hockberger, P.E. (1988). Controlled Outgrowth of Dissociated Neurons on Patterned Substrates. Journal of Neuroscience *8*, 4098-4120.

Koch, S.J., Shundrovsky, A., Jantzen, B.C., and Wang, M.D. (2002). Probing protein-DNA interactions by unzipping a single DNA double helix. Biophysical Journal *83*, 1098-1105.

La Porta, A., and Wang, M.D. (2004). Optical torque wrench: Angular trapping, rotation, and torque detection of quartz microparticles. Physical Review Letters *92*, 190801.

Neuman, K.C., and Block, S.M. (2004). Optical trapping. Rev Sci Instrum *75*, 2787-2809.

Nieminen, T.A., Heckenberg, N.R., and Rubinsztein-Dunlop, H. (2001). Optical measurement of microscopic torques. Journal of Modern Optics *48*, 405-413.

Perkins, T.T. (2009). Optical traps for single molecule biophysics: a primer. Laser Photon Rev *3*, 203-220.

Svoboda, K., and Block, S.M. (1994). Biological Applications of Optical Forces. Annu Rev Biophys Biomolec Struct *23*, 247-285.

CHAPTER 2:

STUDIES OF DNA SUPERCOILING AND PLECTONEME FORMATION USING AN ANGULAR OPTICAL TRAP

* Modified from Physical Review Letters, Volume 100. Forth, S., Deufel, C., Sheinin, M.Y., Daniels, B., Sethna, J.P., and Wang, M.D. *Abrupt Buckling Transition Observed during the Plectoneme Formation of Individual DNA Molecules*. Article 148301, Copyright 2008, with permission from the American Physical Society.

INTRODUCTION

The bending and torsional properties of DNA influence numerous cellular processes, notably DNA compaction, replication, transcription, and protein-DNA binding. DNA elasticity regulates how proteins bend and twist DNA upon binding and how translocating molecular motors exert torque and force on their DNA substrates. Single molecule techniques have proven to be powerful approaches for the investigation of the response of DNA to mechanical stress; individual DNA molecules can be stretched and twisted under physiologically relevant conditions. To date the stretching and bending elasticities of DNA have been well characterized through measurements of the force-extension relation of DNA (Smith et al., 1992; Wang et al., 1997). However, somewhat less is known regarding the torsional elasticity of DNA, at least in part due to difficulties in making direct torque measurements.

The most prevalent method to twist DNA is to use magnetic tweezers to rotate a magnetic bead via rotation of a magnetic field (Crut et al., 2007; Strick et al., 1996). Twisting DNA can also be achieved by rotation of a micropipette cantilever (Leger et al., 1999). These approaches have provided many important insights into DNA torsional properties even without torque detection. A recent and novel technique directly measured torque in DNA via viscous drag force on a small bead attached to the side of a DNA molecule (Bryant et al., 2003). This approach requires taut DNA to minimize writhe and thus is more suited for measurements under high force (> 15 pN). More recently, an angular optical trap that we developed has permitted simultaneous and direct measurements of force and torque for concurrent observation of the tensile and torsional behaviors of DNA over broad ranges of forces and torques (Deufel et al.,

2007; La Porta and Wang, 2004). In addition, its wider bandwidth is well suited for detection of highly kinetic processes.

Previously, our lab has shown that nanofabricated quartz cylinders are ideally suited as handles for angular trapping (see Chapter 1 for a detailed description of the cylinder fabrication). During DNA supercoiling, the torque, angle, force, and extension of a DNA molecule can be simultaneously monitored at kHz rates. In this chapter, I discuss the direct measurement of the torsional modulus of DNA in the intermediate force regime, the determination of basic relations regarding the dependence of torque on applied force, detail the first observation of the abrupt formation of the initial plectoneme (interwound loop) in positively supercoiled DNA, and present previously unseen dynamics of this plectoneme formation.

Additionally, we discovered that previous theoretical treatments of supercoiled DNA could predict the behavior of the molecule before and after the formation of plectonemic coils. However, there had not been an adequate description of the transition itself, which our experimental evidence points to being discontinuous. To this end, we set out to formulate a model which could explain the force and length dependent behavior of the buckling transition. In collaboration with James Sethna and his student Bryan Daniels, a thermodynamic model and elastic rod simulation were developed which make predictions about the nature of the jumps under various conditions, and allow us to visualize what the plectonemic DNA looks like. These theoretical treatments will be briefly discussed near the end of the chapter.

EXPERIMENTAL PROCEDURE

Our angular optical trapping instrument, described in detail in chapter 1, features precise and immediate control of the trapping beam's linear polarization, which is used to rotate a trapped quartz cylinder about its cylindrical axis. The physical torque exerted on the cylinder is determined by direct measurement of the change in angular momentum of the transmitted beam (Bishop et al., 2003; La Porta and Wang, 2004). The quartz cylinders are nanofabricated to ensure uniformity and thus are ideally suited for calibration and measurement reproducibility (Deufel et al., 2007). Each cylinder is also chemically functionalized on one end for specific attachment to DNA.

Here experiments were carried out to measure the response of DNA as it was overwound to introduce positive supercoils. The experimental procedure resembles that previously used for magnetic tweezers studies (Strick et al., 1996), but with the addition of direct torque measurement as we previously described (Deufel et al., 2007). During an experiment as shown in Figure 2.1, a DNA molecule was constrained between the end of a cylinder and the surface of a microscope coverslip, and was held under a constant force (Deufel and Wang, 2006). Subsequently DNA was overwound by steady rotation of the cylinder via rotation of the input laser polarization. During this time, torque, angular orientation, position, and force of the cylinder as well as the location of the coverglass were simultaneously recorded. All experiments were performed in Phosphate Buffered Saline with 150 mM NaCl at 23.5^{o} C.

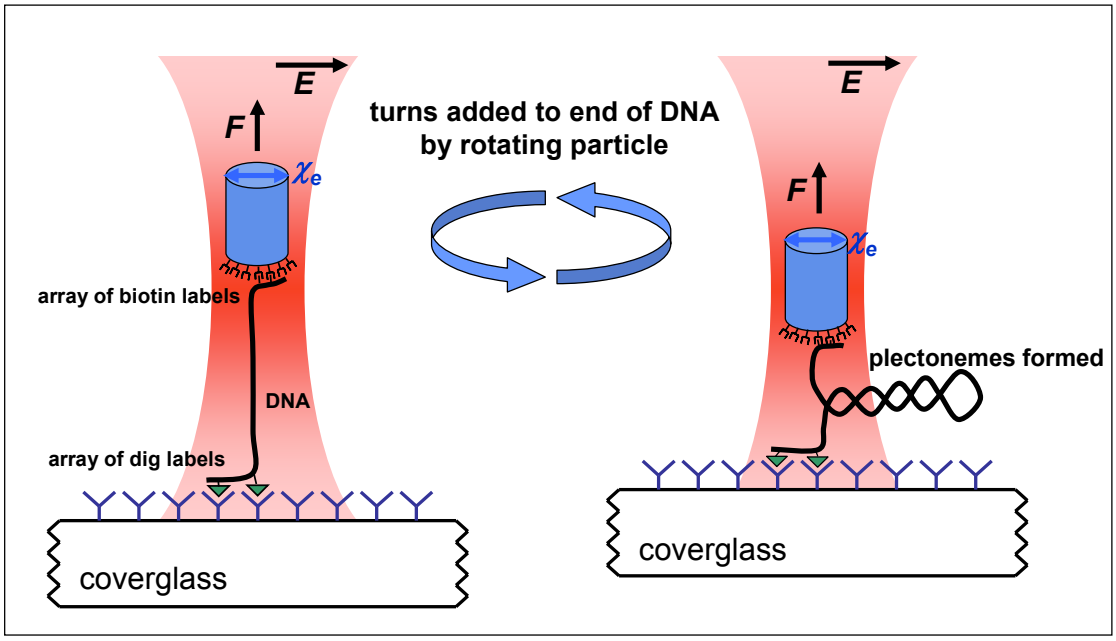

Figure 2.1: Experimental configuration. A DNA molecule was tethered to a nanofabricated birefringent quartz cylinder (extraordinary axis χ_e) held in an angular optical trap. Both ends of the DNA were torsionally constrained via its multiple tags: at one end via biotin-streptavidin and at the other end via digoxigenin (dig) and anti-dig. Force on the cylinder was applied in the axial direction and held constant by feeding back on a piezoelectric stage which displaced the coverslip. The DNA molecule was subsequently overwound by rotation of the linear polarization of the trapping laser.

RESULTS

Figure 2.2 depicts representative single traces of torque and extension as functions of number of turns added to the DNA at three different applied forces. As DNA was overwound at 1 turn/s, torque increased linearly while the extension remained approximately constant. This continued until the DNA buckled to form a plectoneme, indicated by a sudden decrease in extension. The buckling transition arises when the free energy of the extended DNA becomes larger than that of the initial plectonemic structure within the DNA. Beyond this transition, with additional twist the plectonemic region was extended continuously while the end-to-end extension decreased linearly and the torque plateaued at a constant value. Note that the torque and the extension slope after buckling were strongly sensitive to applied tension in the DNA.

Additional experiments were carried out to verify that the data were taken under quasi-equilibrium conditions; when the supercoiled DNA was relaxed at the same rotation rate, the data were essentially indistinguishable. An example of this phenomenon is presented in Figure 2.3, which shows a single DNA molecule held at 2 pN overwound past the buckling transition and, upon the addition of 20 turns, is immediately unwound at the same rate. Note that all important features, including the location of the DNA buckling event and the onset of the phase transition, are indistinguishable, indicating the system is approximately in equilibrium.

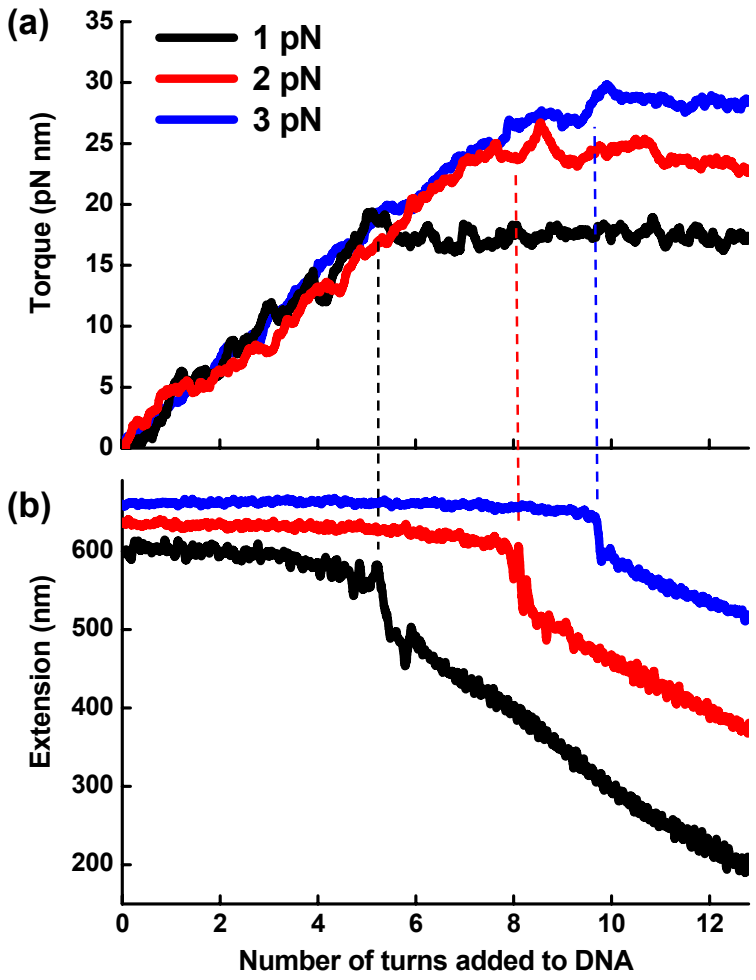

Figure 2.2: Examples of torque and extension versus turn number. DNA molecules of 2.2 kbp in length were overwound under a constant force. Data were collected at 2 kHz and averaged with a sliding window of 1.5 s for torque and 0.05 s for extension (the torque signal had more Brownian noise relative to signal and was thus subjected to this higher degree of filtering). As a result, higher frequency features in the torque signal, especially those near the buckling transition, have been obscured. DNA buckling, locations indicated by dashed lines, was dependent on the applied force. (a) Torque versus number of turns. (b) The corresponding extension versus number of turns.

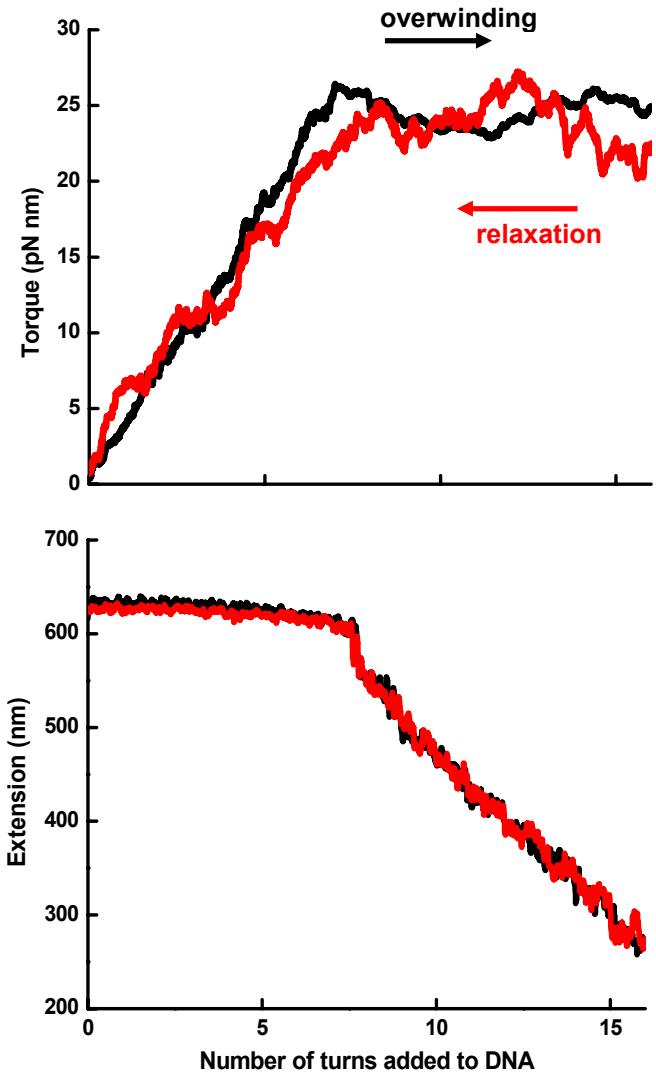

Figure 2.3: Reversibility of over-winding DNA. A 2.2 kbp DNA molecule was held at a constant force of 2 pN and overwound by 20 turns at a rate of 1 turn/s. Winding direction was immediately reversed at the same rate to return the DNA to its torsion-free state. The over-winding and its reversal yielded overlapping data traces for both the extension and torque signals, indicating the measurements were carried out under quasi-equilibrium conditions.

One of the most significant features of the overwinding data in Figure 2.2.b is the pronounced sharp drop in extension at the buckling transition, corresponding to the formation of the initial plectoneme. Interestingly, such an abrupt transition was absent in previous magnetic tweezers measurements where instead a smooth and gradual transition was observed (Strick et al., 1996). The angular trapping method allowed detection of the abrupt transition, likely due to higher bandwidth and increased spatial resolution together with the use of shorter DNA tethers.

As shown in Figure 2.4, the magnitude of the extension drop observed at the buckling transition was dependent on the applied force, following a power law of $\sim F^{-0.5}$. In contrast, the extension decrease per turn after the transition followed a power law of $\sim F^{-0.4}$, as observed in previous magnetic tweezers studies (Strick et al., 2003). Furthermore, the first loop of the plectoneme was able to absorb approximately twice as much extension as was absorbed into the plectoneme upon each additional single turn. These two distinct regimes of extension change versus force are depicted in Figure 2.4.

In addition, three different DNA templates were used for these experiments: a 2.2 kbp DNA, a 4.2 kbp DNA containing the 2.2 kbp sequence, and a 2.2 kbp DNA with a sequence entirely different from the first two. The extension changes were found to be the same for all three DNA templates, indicating that they are neither length nor sequence dependent within the limits of our measurements.

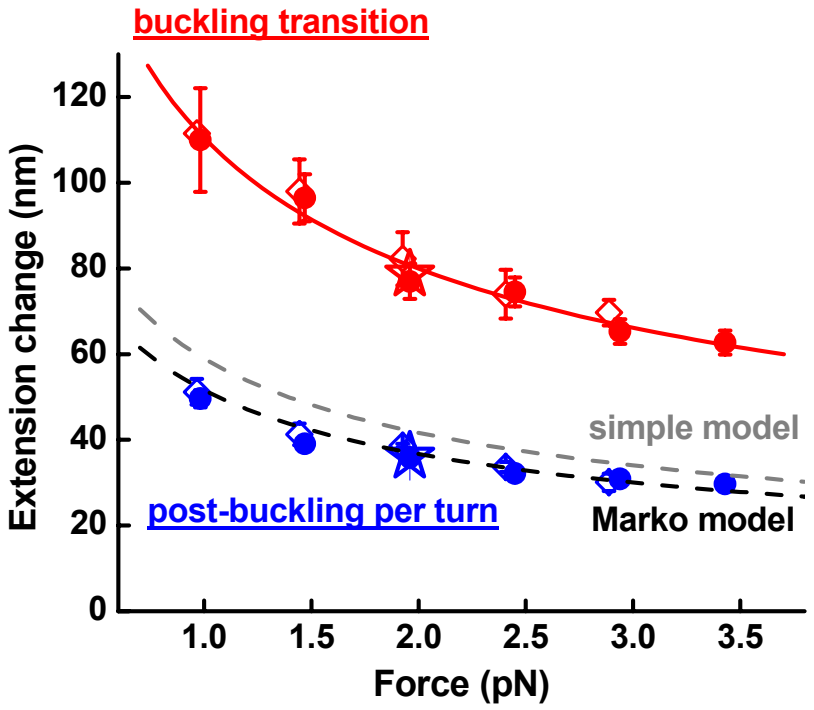

Figure 2.4: Extension change at the buckling transition versus force. The extension change for the initial plectoneme loop (red symbols) was well fit by a power law of $F^{-0.5\pm0.02}$ (solid red) and was much larger than the extension change per turn for subsequent plectoneme growth (blue symbols). Three different DNA templates (2.2 kbp •, N = 119; 4.2 kbp ◊, N = 35; another 2.2 kbp ★, N = 4) all exhibited the same trend. The two dashed lines show predictions by a simple model and a fit to the Marko model respectively, using the independently measured value of C and L_p, and free parameter P. Error bars are standard errors of the means.

Data from Figure 2.2 suggest that the energy barrier between the extended and plectonemic states is low enough for transitions between the two states to occur at an observable rate. To test this idea, a DNA tether was overwound extremely slowly through the buckling transition (Figure 2.5). The extension of the DNA was observed to fluctuate between two discrete states, corresponding to pre- and post-buckling. The rates of fluctuation were highly sensitive to twist and we estimate that they were on the order of ~ 10 Hz near the rotational mid-point of the transition. The two states were separated by 79 nm, in good agreement with the extension drop observed at the same force in the rapid winding experiment in Figure 2.4. It should be noted that this dynamic process can not be observed with current magnetic tweezers technology, due to the limited bandwidth of that technique (<1 Hz), and demonstrates one major advantage that our new technology has.

Measurements like those shown in Figure 2.2 allowed direct determination of the torsional modulus of DNA. We plotted torque-turn relations by pooling the torque data taken at various forces prior to buckling for either the 2.2 kbp or 4.2 kbp tethers (Figure 2.6). Prior to buckling, DNA may be modeled as a simple elastic torsional rod. As twist is applied to the DNA, the restoring torque τ will increase linearly with the twist angle, as given by: $\tau = C\frac{2\pi n}{L_0}$, where L_0 is the contour length of the rod with 1 bp corresponding to 0.34 nm, n is the number of turns added, and C is the torsional modulus. The slopes of the measured torque-turn relations yielded a torsional modulus of $C = 90 \pm 3$ nm k_BT (88 ± 4 nm k_BT) for the 2.2 kbp (4.2 kbp) DNA, corresponding to an intrinsic torsional modulus of ~100 nm k_BT (Moroz and Nelson, 1997). Previous studies, which have employed techniques such as DNA cyclization (Horowitz and Wang, 1984), fluorescence polarization anisotropy (Selvin et al., 1992),

or magnetic tweezers (Strick et al., 1999), have reported values ranging from 50 to 120 nm k_BT for various temperature and buffer conditions. Our measured twist persistence length $\frac{C}{k_BT}$ of ~ 90 nm corresponds to a true twist persistence length of ~100 nm in the absence of bending fluctuations.

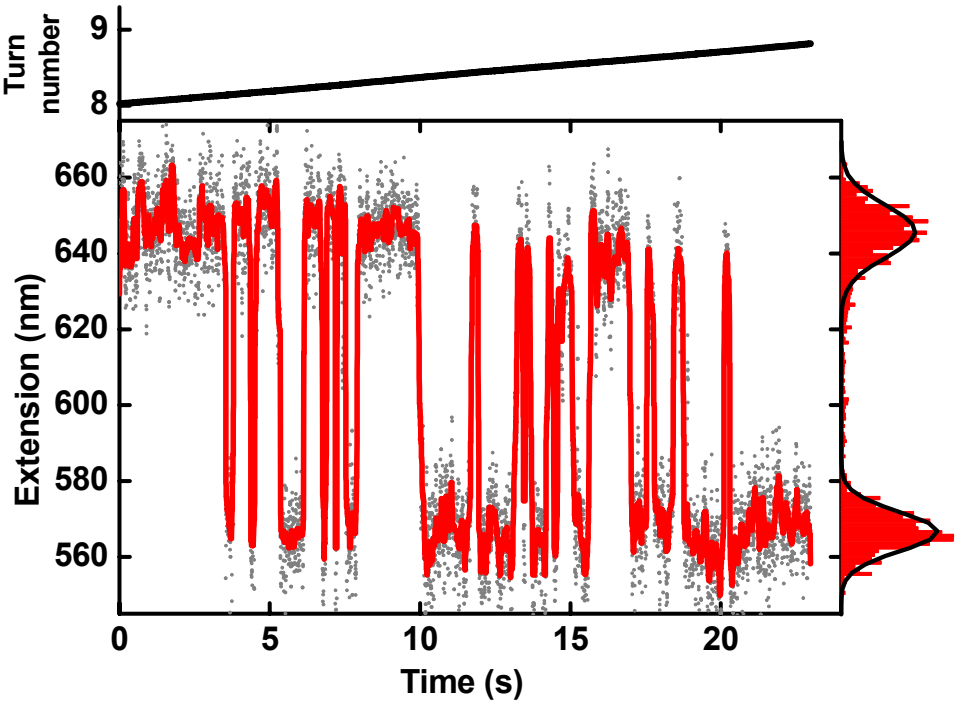

Figure 2.5: A 2.2. kbp molecule was held at constant tension (2 pN) and overwound extremely slowly (0.04 turn/s) through its buckling transition. Data were taken at 2 kHz, low pass filtered to 400 Hz (solid dots), and then median filtered to 20 Hz (red curve). An extension histogram of the median-filtered data is shown on the right and was well fit by the sum of two Gaussians (black curve). The DNA was observed to rapidly fluctuate between two distinct states, separated by 79 nm, corresponding to pre- and post-formation of the first plectonemic loop.

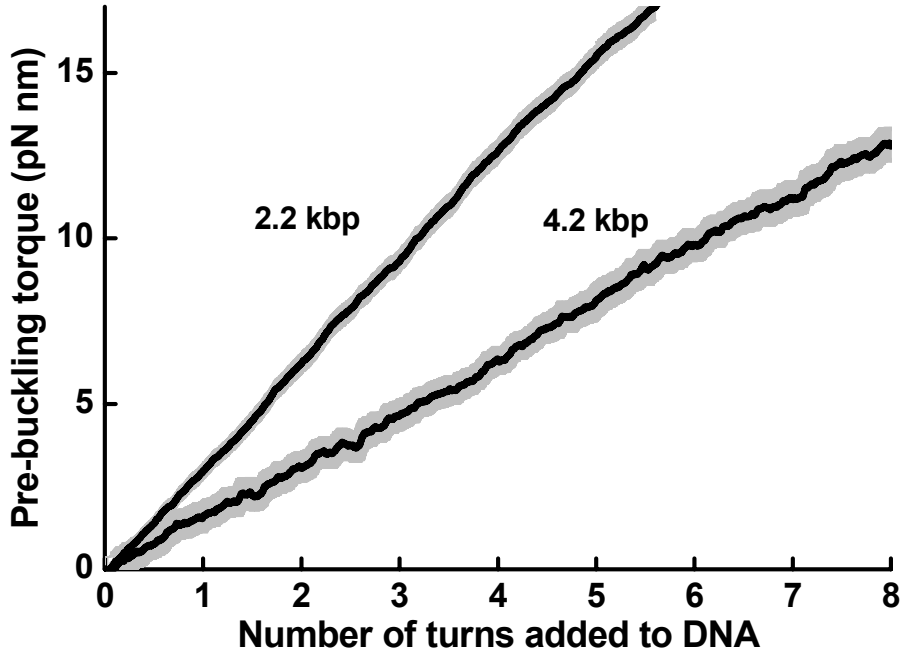

Figure 2.6: Direct measurements of torque prior to the buckling. Torque-turn relations prior to buckling were pooled from data for both the 2.2 kbp DNA (121 traces) and 4.2 kbp DNA (65 traces). Individual traces are shown as grey lines and resulted in a grey region when plotted together. Each solid curve indicates the average of all traces of a given length DNA. Torsional modulus for each DNA length (see text for values) was obtained by the slope of a linear fit to the average curve.

These measurements also allow direct determination of the post-buckling torque. Figure 2.7 summarizes data for post-buckling torque versus force for all three DNA templates. The post-buckling torque increased with force and was independent of DNA length and sequence.

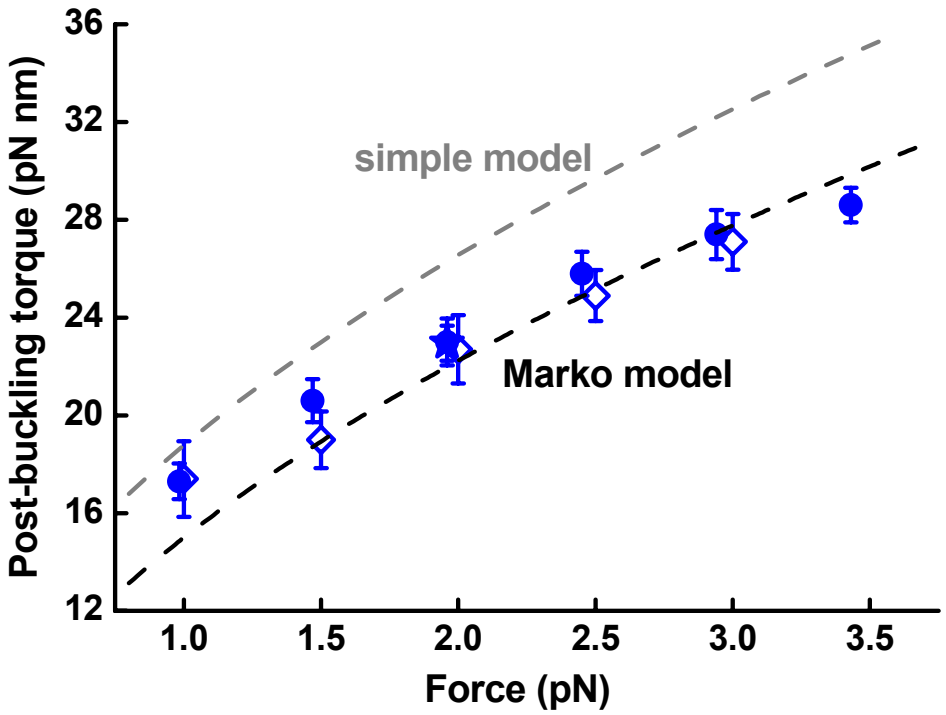

Figure 2.7: Torque after buckling. The torque after buckling at each force was pooled from data from the three DNA templates (blue symbols: 2.2 kbp ●, N = 119; 4.2 kbp ◊, N = 35; another 2.2 kbp★, N = 4). The two dashed lines show predictions by the simple model and a fit to the Marko model respectively.

THEORETICAL PREDICTIONS

A number of models exist to explain DNA properties post-buckling. A simple model treats DNA as an elastic rod and assumes that a plectoneme consists of circular loops, predicting an extension change per turn after buckling of $\Delta z = \pi\sqrt{\frac{2L_p k_B T}{F}}$ and a post-buckling torque given by $\tau_c = \sqrt{2L_p k_B T F}$, where L_p is the persistence length of the DNA, $k_B T$ is the thermal energy, and F is the applied force. We carried out force-extension measurements similar to those described before (Wang et al., 1997) and determined $L_p = 43 \pm 3$ nm under our experimental conditions. The predicted post-buckling extension change per turn and post-buckling torque versus force, shown Figures 2.4 and 2.7 respectively are greater than measurements by as much as 25%.

Several more elaborate models exist to describe DNA supercoiling analytically (Bouchiat and Mezard, 1998; Marko, 2007; Purohit and Nelson, 2007). In particular, an elegant recent theoretical work by John Marko (Marko, 2007) employed a detailed statistical mechanics analysis to incorporate an effective torsional flexibility of the plectonemic state (plectonemic rigidity) (Vologodskii et al., 1992) and a force-dependent torsional flexibility of the extended state (Moroz and Nelson, 1997). This model, which we refer to here as the Marko model, provides closed-form expressions for both the extension change per turn and the post-buckling torque.

To derive the expected change in extension after the buckling transition, we consider the following, derived from Marko, PRE 021926, 2007. The following abbreviations and shorthand are employed during these calculations:

Notation:

Variables:

$F \equiv$ force.

$L_p \equiv$ bending persistence length.

$C \equiv$ twist persistence length (straight DNA segment).

$P \equiv$ plectoneme twist persistence length (plectonemic DNA segment).

$k_B T \equiv$ thermal energy.

$3.57nm \equiv$ helical pitch of DNA.

Derived Relations/Expressions:

$$\omega_0 \equiv (2\pi / 3.57) nm^{-1}$$

$$c \equiv k_b T C \omega_0^{\ 2}$$

$$p \equiv k_b T P \omega_0^{\ 2}$$

$$c_s \equiv c\left(1 - \frac{C}{4L_p}\sqrt{\frac{k_b T}{F L_p}}\right)$$

$$g \equiv F - \sqrt{\frac{k_b T F}{L_p}}$$

Extension (as a fraction of relaxed double helix contour length L, equation 5) can be written as:

$$\frac{z}{L} = -\frac{\partial F}{\partial f}$$

where F is the free energy and f is force.

Considering the free energy of the molecule before buckling (equation 9),

$$F = S(\sigma) = -g + \frac{c_s}{2}\sigma^2$$

and, taking the derivative:

$$\frac{z}{L} = 1 - \frac{1}{2}\sqrt{\frac{kT}{fA}} - \frac{\omega_0^2 C^2}{16}\left(\frac{kT}{Af}\right)^{3/2}\sigma^2$$

By means of the double tangent construction, one can see that the fractions of stretched and plectonemic states (x_s and x_p) during the phase coexistence depends linearly on the linking number density. As the plectonemic state has zero length, extension may be written as (equation 6):

$$\frac{z}{L} = x_s \frac{z(\sigma_s)}{L} = \frac{\sigma_p - \sigma}{\sigma_p - \sigma_s}\frac{z(\sigma_s)}{L}$$

where σ_s and σ_p are linking number densities at the beginning and at the end of the transition, and $z(\sigma_s)$ is the extension at the beginning of the transition.

It is possible to express the previous formula in terms of known parameters (equation 14).

Therefore, the slope of extension (as a fraction of contour length L) versus linking number is:

$$\frac{\partial(z/L)}{\partial\sigma} = -\frac{z(\sigma_s)/L}{\sigma_p - \sigma_s} = \frac{\left[1 - \frac{1}{2}\sqrt{\frac{kT}{fA}} - \frac{\omega_0^2 C^2}{16}\left(\frac{kT}{Af}\right)^{3/2}\sigma_s^2\right]}{\sigma_p - \sigma_s}$$

$$= \frac{\left[1 - \frac{1}{2}\sqrt{\frac{kT}{fA}} - \frac{\omega_0^2 C^2}{16}\left(\frac{kT}{Af}\right)^{3/2}\left(\frac{1}{c_s}\sqrt{\frac{2pg}{1-p/c_s}}\right)^2\right]}{\sqrt{\frac{2pg}{1-p/c_s}}\left(\frac{1}{p} - \frac{1}{c_s}\right)}$$

Above quantity is dimensionless. To convert into nm/turn, note that each turn changes the DNA linking number by one, therefore changing the linking number density by $\frac{1}{Lk_0}$, where $Lk_0 = \frac{L(nm)}{3.57(nm)}$ is the initial linking number. So, slope in nm/turn is given by:

$$\Delta z = \frac{(3.57nm)\left[1 - \frac{1}{2}\sqrt{\frac{k_B T}{FL_p}} - \frac{\omega_0^2 C^2}{16}\left(\frac{k_B T}{FL_p}\right)^{3/2}\left(\frac{1}{c_s}\sqrt{\frac{2pg}{1-p/c_s}}\right)^2\right]}{\sqrt{\frac{2pg}{1-p/c_s}}\left(\frac{1}{p} - \frac{1}{c_s}\right)}.$$

Similarly, the predicted torque after buckling (Marko, PRE 021926, 2007, equation 17):

$$\tau_c = \sqrt{\frac{2k_B TPg}{1 - P/C}}.$$

All parameters in the model were experimentally determined in this work, except for the plectonemic rigidity. We therefore performed a global fit of our measurements to the model using the plectonemic rigidity as the single fit parameter. The resulting best

fit for the extension change per turn was in excellent agreement with the measurements (Figure 2.4) and the resulting best fit for the post-buckling torque agreed with the measurements to within 15% (Figure 2.7). In addition, the best fit value for the plectonemic rigidity was 26 nm, within the range of 21- 27 nm as previously estimated (Vologodskii et al., 1992).

Prior to this work, we were not aware of any analytical models suitable for prediction of the observed extension change and dynamics at the buckling transition. Mechanical rod simulations should be extendable to explain DNA supercoiling; for instance, Goyal et al. formulated a non-linear dynamic rod simulation which shows an abrupt buckling followed by subsequent formation of a loop in a macroscopic rod (Goyal et al., 2008), a prediction that bears resemblance to our measurements. However, the lack of an adequate and useful *analytical* model describing the supercoiling transition itself has led to the development of a theoretical treatment by Bryan Daniels in a collaboration between the labs of James Sethna and Michelle Wang (Daniels et al., 2008).

In formulating a model, the two regimes of interest must be considered: the "stretched state" (SS, prior to plectoneme formation) and "coexisting state" (CS, both plectonemes and straight DNA coexisting), both of which have been previously and independently explored. The worm-like chain model for a fluctuating polymer has been successfully employed to describe the behavior of non-plectonemic DNA (Marko and Siggia, 1995). Plectonemic DNA, which stores excess torsional energy as writhe, has similarly been modeled, as detailed earlier in this chapter (Marko, 2007). It is the discontinuity at the transition between the two states which deserves further attention and for which theoretical treatments have been lacking.

The data presented previously in this chapter depicts an abrupt extension change, Δz, at the transition between the SS and CS states which is, within measurement error, independent of the length of DNA for the two lengths (2.2 kbp and 4.2 kbp) tested. It is not intuitively obvious that this extension change should be independent of length, though the inclusion of entropic effects significantly reduces the length dependence. Because the extension features a sharp discontinuity, the torque should also undergo a similar jump, Δτ. Due to the high degree of filtering applied to the noisy torque signal, no such jump was readily observed in the fast winding data. However, by parsing and averaging the data at the transition during the slow winding experiment, we can extract a value of Δτ at a particular force and DNA length, and we will find that it agrees well with theoretical predictions. It is therefore the goal of Daniels' theoretical treatment to formulate a model by which the magnitudes of the extension and torque jumps can be predicted for many forces and DNA lengths.

The SS has been well described by the free energy term:

$$F_{SS}(K,L) = \frac{C}{2}\left(2\pi\frac{K}{L}\right)^2 L - F_{eff}L$$

where K is the additional linking number, L is the total length of the DNA, C is the torsional modulus (measured as 89 +/- 3 nm-kT earlier in this work) and $F_{eff} = F - kT\sqrt{\frac{F}{B}}$, where F is the force applied to the molecule ends and B is the bending elastic constant, measured as 43 +/- 3 nm-kT in a separate experiment. By differentiating with respect to K, we can derive the torque, $\tau_{SS} = 2\pi C\frac{K}{L}$ (an identical expression to that discussed previously). The extension of DNA undergoing thermal fluctuations can be written as $z_{SS} = \xi(\tau_{SS})L$, where

$$\xi(\tau) = 1 - \frac{1}{2}\left[\frac{BF}{(kT)^2} - \left(\frac{\tau}{2kT}\right)^2 - \frac{1}{32}\right]^{-\frac{1}{2}}$$ (Moroz and Nelson, 1998).

Motivated by the method of the double-tangent construction from Marko, Daniels observes that the free energy and extension jump in the CS state are linear functions of both K and L, and derives the following expressions:

$$F_{CS}(K,L) = F_0 + 2\pi\tau K - \left(\frac{\tau^2}{2C} + F_{eff}\right)L$$

$$z_{CS}(K,L) = -z_0 - qK + \left(\xi(\tau) + \frac{\tau}{2\pi C}q\right)L\,.$$

Employing the available experimental data from the CS, Daniels is able to extract the slopes τ and q, as well as the K=L=0 intercepts F_0 and z_0 as functions of external tension. By balancing the free energy between the SS and CS states, expressions for the critical transition turn number K^* and the extension jump Δz can be derived:

$$K^* = \frac{L}{2\pi C}(\tau + \Delta\tau) = \frac{L}{2\pi C}\left(\tau + \sqrt{\frac{2C}{L}F_0}\right)$$

$$\Delta z = z_0 + q\sqrt{\frac{LF_0}{2\pi^2 C}} - L\left(\xi(\tau) - \xi\left(\tau + \sqrt{\frac{2CF_0}{L}}\right)\right).$$

Daniels numerically simulated the buckling of an elastic rod under tension and torsional strain, taking into account the self repulsion of two segments coming into close contact, a physically real effect which arises from both Coulomb screening interactions and loss of entropy within the tightly packed plectoneme structure. This approach yielded values for the extension jump which did not agree well with

measurements at low forces, and were highly dependent on the length of the DNA. By combining the analytical approach above with experimental observables, the predictions bore closer resemblance to the experimental data. Finally, after considering entropic effects, Daniels found that the strong length dependence of the simulation nearly disappeared, and found the analytical approach was able to make good predictions about the behavior of buckling DNA. Further experimentation on even more lengths of DNA and over a wider range of forces could serve to refine the model even further. Additionally, as the analytical framework incorporates more and more physically real phenomenon (entropic effects, sequence dependence, localized DNA kinking), it is believed that the ability to predict plectoneme formation behavior will become even more enhanced.

Importantly, the theory predicts a torque jump on the order of 3-4 pN-nm at the transition for the lengths of DNA and forces used in these experiments. Direct observation of the torque jump can be difficult, owing to the high degree of Brownian noise intrinsic to the system. Time averaging helps to minimize this effect, but taking data for too long results in error as well, as the measurement system is highly susceptible to low frequency mechanical drift (of either the coverslip mounting apparatus, or the microscope objective itself). Thus, there is a desired measurement regime; long enough to acquire adequate data for averaging, but fast enough to eliminate the effects of mechanical or thermal drift. This regime is, in practice, in the 0.1 to 1 Hz range used in these experiments, and the torque signals presented above are thusly sufficiently averaged to provide useful equilibrium torque data. The torque jump however is, by its nature, sudden and therefore very fast, so measurement of this small change in signal has proven difficult. That being said, it is possible to extract a value by separately averaging the SS and CS torque data at the transition hopping

regime, as shown in Figure 2.8. In this case, the extension data provides a clear guide by which we can determine those portions of the torque data that correspond to the upper SS state and those which belong to the CS state. It is apparent that the data taken herein consists of enough points to provide a useful mean value, while maintaining the nature of the rapid fluctuations. By parsing these two regimes, with the extension data as the guide, we can subsequently average the torque signal from each and find the difference. From this data analysis method, we extract a torque jump of 2.9 +/- 0.7 pN-nm, in good agreement with the theoretical prediction (at 2 pN for 2.2 kbp DNA) of 3.9 +/- 2.6 pN-nm.

The treatment of Daniels has also been used to describe the nature of the end loop formed during the buckling event. It was found that describing the loop as circular does not fit as well as a shallower, more teardrop-like shape; this is confirmed in the numerical simulation as well. In general, this formulation is capable of predicting the expected amount of DNA to be absorbed into the loop, regardless of its geometry, and future improvements could refine it even more. For instance, allowing for multiple plectonemes, alternate geometries, or sequence dependent elastic parameters could all allow for more accurate fits with the experimental data and provide a robust method by which DNA supercoiling can be studied.

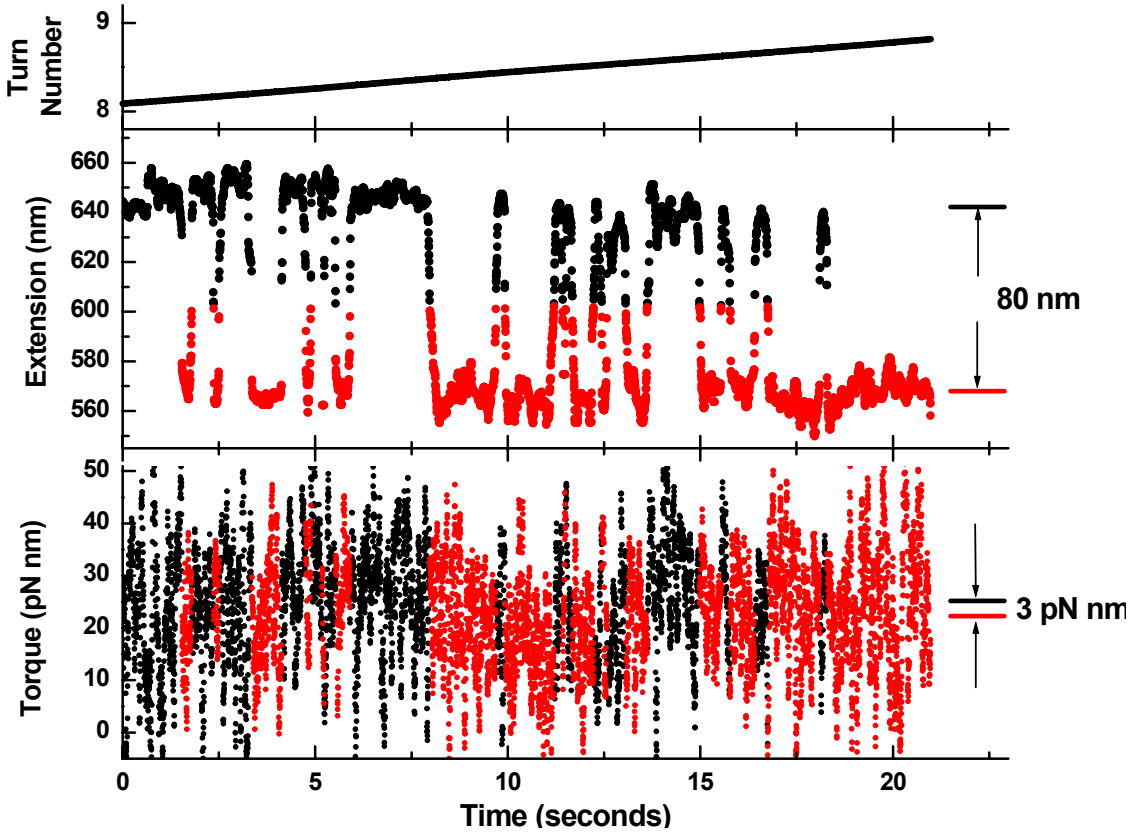

Figure 2.8: Extracting the torque jump from the plectoneme hopping data. The slow winding experiment data was parsed into two segments; that belonging to the SS state (black points) and CS (red points). The mean torque value for all data in each condition was averaged, and allowed for the determination of the magnitude of the torque jump. The torque jump $\Delta\tau$ was found to be ~3 pN-nm, in excellent agreement with theoretical predictions at this force and DNA length.

CONCLUSIONS

The highly dynamic nature of a twisted DNA molecule at the buckling transition may have important biological consequences in vivo. The specific supercoiling density (0.00 - 0.10) and applied force (1.0 - 3.5 pN) are well within the range commonly experienced by DNA in the cell. If a DNA molecule is subject to moderate stresses, distant elements on the sequence may transiently be brought into contact, which may facilitate the binding of DNA looping proteins or transcription factors (Nelson, 1999). The rapid formation and loss of these transient loops could therefore greatly reduce the search time needed for a protein to find two spatially separated sequence elements on the template.

Direct measurements of DNA torsional response lays an important foundation for the understanding of many biological processes that are regulated by torque. For example, topoisomerases are known to mediate linking numbers in DNA by sensing torsional stress in the DNA (Koster et al., 2005). RNA polymerases as well as other groove-tracking enzymes are expected to rotate about the DNA helical axis (Harada et al., 2001; Revyakin et al., 2006), and would thereby generate and move against positive torque in the downstream DNA. We anticipate major progress in these areas with the advent of a number of biophysical techniques (including the one presented here) to measure and control the rotation of microscopic particles (Bishop et al., 2004; Bryant et al., 2003; Deufel et al., 2007; Oroszi et al., 2006). The angular optical trap, with its wide bandwidth, high spatial resolution, and ability to simultaneously measure force and torque, should prove to be a valuable tool to understand these highly kinetic and mechanical processes.

REFERENCES

Bishop, A.I., Nieminen, T.A., Heckenberg, N.R., and Rubinsztein-Dunlop, H. (2003). Optical application and measurement of torque on microparticles of isotropic nonabsorbing material. Phys Rev A *68*, 033802.

Bishop, A.I., Nieminen, T.A., Heckenberg, N.R., and Rubinsztein-Dunlop, H. (2004). Optical microrheology using rotating laser-trapped particles. Physical Review Letters *92*, 198104.

Bouchiat, C., and Mezard, M. (1998). Elasticity model of a supercoiled DNA molecule. Physical Review Letters *80*, 1556-1559.

Bryant, Z., Stone, M.D., Gore, J., Smith, S.B., Cozzarelli, N.R., and Bustamante, C. (2003). Structural transitions and elasticity from torque measurements on DNA. Nature *424*, 338-341.

Crut, A., Koster, D.A., Seidel, R., Wiggins, C.H., and Dekker, N.H. (2007). Fast dynamics of supercoiled DNA revealed by single-molecule experiments. Proc Natl Acad Sci U S A *104*, 11957-11962.

Daniels, B.C., Forth, S., Sheinin, M.Y., Wang, M.D., and Sethna, J.P. (2008). Discontinuities at the DNA supercoiling transition. arXiv, 0811.3645v0811.

Deufel, C., Forth, S., Simmons, C.R., Dejgosha, S., and Wang, M.D. (2007). Nanofabricated quartz cylinders for angular trapping: DNA supercoiling torque detection. Nat Methods *4*, 223-225.

Deufel, C., and Wang, M.D. (2006). Detection of forces and displacements along the axial direction in an optical trap. Biophysical Journal *90*, 657-667.

Goyal, S., Perkins, N.C., and Lee, C.L. (2008). Non-linear dynamic intertwining of rods with self-contact. Int J Non-Linear Mech *43*, 65-73.

Harada, Y., Ohara, O., Takatsuki, A., Itoh, H., Shimamoto, N., and Kinosita, K. (2001). Direct observation of DNA rotation during transcription by Escherichia coli RNA polymerase. Nature *409*, 113-115.

Horowitz, D.S., and Wang, J.C. (1984). Torsional Rigidity of DNA and Length Dependence of the Free-Energy of DNA Supercoiling. Journal of Molecular Biology *173*, 75-91.

Koster, D.A., Croquette, V., Dekker, C., Shuman, S., and Dekker, N.H. (2005). Friction and torque govern the relaxation of DNA supercoils by eukaryotic topoisomerase IB. Nature *434*, 671-674.

La Porta, A., and Wang, M.D. (2004). Optical torque wrench: Angular trapping, rotation, and torque detection of quartz microparticles. Physical Review Letters *92*, 190801.

Leger, J.F., Romano, G., Sarkar, A., Robert, J., Bourdieu, L., Chatenay, D., and Marko, J.F. (1999). Structural transitions of a twisted and stretched DNA molecule. Physical Review Letters *83*, 1066-1069.

Marko, J.F. (2007). Torque and dynamics of linking number relaxation in stretched supercoiled DNA. Phys Rev E *76*, 021926.

Marko, J.F., and Siggia, E.D. (1995). Stretching DNA. Macromolecules *28*, 8759-8770.

Moroz, J.D., and Nelson, P. (1997). Torsional directed walks, entropic elasticity, and DNA twist stiffness. Proc Natl Acad Sci U S A *94*, 14418-14422.

Moroz, J.D., and Nelson, P. (1998). Entropic elasticity of twist-storing polymers. Macromolecules *31*, 6333-6347.

Nelson, P. (1999). Transport of torsional stress in DNA. Proc Natl Acad Sci U S A *96*, 14342-14347.

Oroszi, L., Galajda, P., Kirei, H., Bottka, S., and Ormos, P. (2006). Direct measurement of torque in an optical trap and its application to double-strand DNA. Physical Review Letters *97*, 058301.

Purohit, P.K., and Nelson, P.C. (2007). Effect of supercoiling on formation of protein-mediated DNA loops (vol 74, art no 061907, 2006). Phys Rev E *75*, 039903.

Revyakin, A., Liu, C.Y., Ebright, R.H., and Strick, T.R. (2006). Abortive initiation and productive initiation by RNA polymerase involve DNA scrunching. Science *314*, 1139-1143.

Selvin, P.R., Cook, D.N., Pon, N.G., Bauer, W.R., Klein, M.P., and Hearst, J.E. (1992). Torsional Rigidity of Positively and Negatively Supercoiled DNA. Science *255*, 82-85.

Smith, S.B., Finzi, L., and Bustamante, C. (1992). Direct Mechanical Measurements of the Elasticity of Single DNA-Molecules by Using Magnetic Beads. Science *258*, 1122-1126.

Strick, T.R., Allemand, J.F., Bensimon, D., Bensimon, A., and Croquette, V. (1996). The elasticity of a single supercoiled DNA molecule. Science *271*, 1835-1837.

Strick, T.R., Bensimon, D., and Croquette, V. (1999). Micro-mechanical measurement of the torsional modulus of DNA. Genetica *106*, 57-62.

Strick, T.R., Dessinges, M.N., Charvin, G., Dekker, N.H., Allemand, J.F., Bensimon, D., and Croquette, V. (2003). Stretching of macromolecules and proteins. Rep Prog Phys *66*, 1-45.

Vologodskii, A.V., Levene, S.D., Klenin, K.V., Frankkamenetskii, M., and Cozzarelli, N.R. (1992). Conformational and Thermodynamic Properties of Supercoiled DNA. Journal of Molecular Biology *227*, 1224-1243.

Wang, M.D., Yin, H., Landick, R., Gelles, J., and Block, S.M. (1997). Stretching DNA with optical tweezers. Biophysical Journal *72*, 1335-1346.

CHAPTER 3:

A BIOLOGICAL NANO-TORQUE WRENCH: MECHANICAL STUDIES OF THE HOLLIDAY JUNCTION

INTRODUCTION

DNA structure is modulated dynamically throughout the cell cycle via mechanical stress exerted by motor enzymes and DNA binding proteins. A DNA molecule assumes a B-form structure when relaxed but can undergo phase transitions to other structures upon stretching and twisting. Direct measurements of the biological torques involved have proven to be much more challenging than measurements of their force counterparts. In this chapter are presented the smallest biological torques directly measured to date. It was found that the torque required to mechanically migrate a Holliday junction is at least ten times smaller than that required to melt dsDNA (Strick et al., 1999) or to induce dsDNA buckling (Forth et al., 2008). These observations set a new scale for what may be considered to be physiologically relevant torque and suggest a mechanism for dissipation of torsional stress which can accumulate during many biological processes.

The four-way Holliday junction is an important nanoscopic DNA structure in vivo, formed during homologous recombination (Kowalczykowski et al., 1994), double stranded break repair (van Gent et al., 2001), replication fork recovery (Courcelle and Hanawalt, 2003), and at inverted repeat sequences (Pearson et al., 1996). Holliday junction migration may be enzymatically mediated by molecular motors or junction binding proteins (Dawid et al., 2004), which have been shown to use ATP hydrolysis to bias the random walk state of Holliday junction for directional branch migration (Rasnik et al., 2008). Even in the absence of motor enzymes, branch migration may take place spontaneously due to a low energetic cost for migration because the nearly fully base-paired DNA structure is preserved during this process except at the junction (Panyutin and Hsieh, 1994). The application of a tension along opposing DNA trunks

of the Holliday junction, therefore, should result in a biased junction migration to extend the trunks and a simultaneous rotation of the DNA ends. However, if the ends of the DNA trunks are not free to rotate, a torque will arise to oppose the junction migration, preventing further junction migration.

Here we employed an angular optical trap (La Porta and Wang, 2004) to mechanically migrate individual Holliday junctions. A palindromic DNA molecule of total length 2.2 kbp with a pre-formed Holliday junction at its midpoint was torsionally constrained at both ends and held under a fixed force using an angular optical trap. The Holliday junction was then migrated by rotation of a trapped nanofabricated quartz cylinder (Deufel et al., 2007): for each left-handed full turn of the cylinder, the DNA extension decreased by approximately 3.4 nm, as the DNA was converted from the top and bottom trunks to the two side arms. The migration was smooth and fully reversible as evidenced by the extension signal, indicating the system was under thermodynamic quasi-equilibrium. Previous studies on cruciform extrusion using magnetic tweezers yielded similar extension behavior (Dawid et al., 2006), but that technique does not allow for direct torque measurement. With the ability of our instrument to directly monitor the torque exerted on the cylinder by the junction itself, we were able to determine the relation between applied tension and that torque. We found that the results agreed very well with a simple thermodynamic prediction, and present the derivation near the end of this chapter. Finally, the biological implication for such a small torque required to stabilize the junction are discussed.

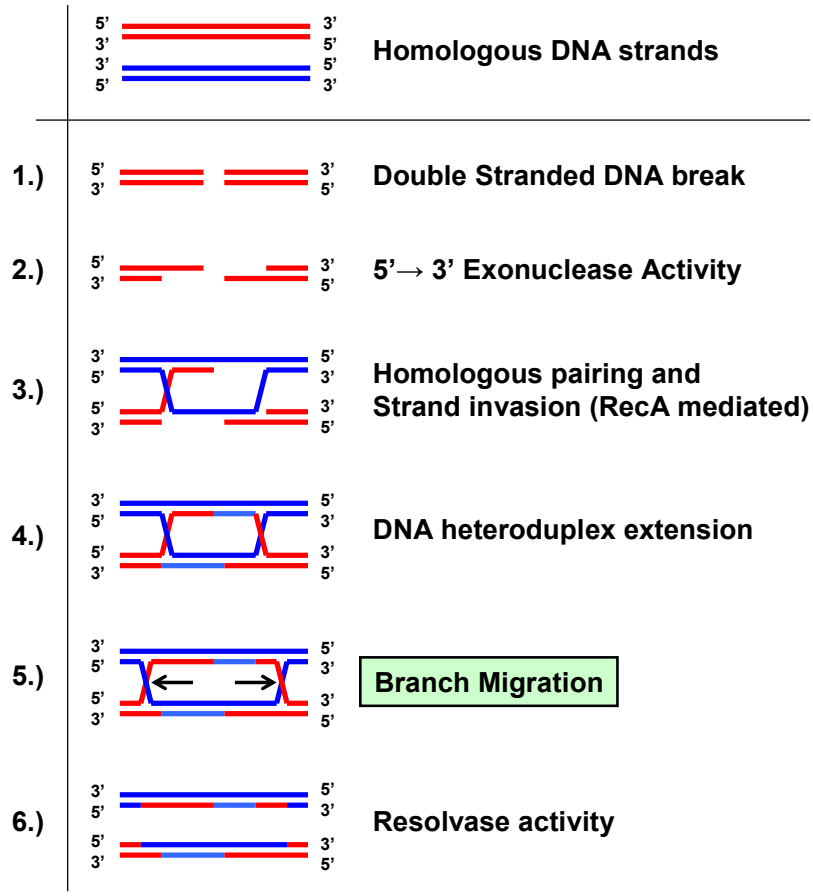

Figure 3.1: A model for homologous recombination mediated DNA repair. Upon the breakage of one dsDNA segment (1), the homologous recombination repair pathway is initiated. First, 3' overhangs are generated by the action of an exonuclease (2). The single stranded DNA is loaded with a RecA (or RecA homolog) forming a filament, which promotes homologous pairing via strand invasion of an identical segment of DNA (3). The DNA heteroduplex is extended via the action of a DNA polymerase (4). The resulting product consists of multiple Holliday junctions, which may be subsequently branch migrated (5). Upon arrival at particular identification sequences, the junctions are resolved (6), resulting in two full heteroduplex structures, thus completing the recombination or HR mediated DNA repair pathway.

HOMOLOGOUS RECOMBINATION AND dsDNA BREAK REPAIR

Homologous recombination is an important process occurring during many parts of the cell cycle. It is a primary pathway for double stranded DNA break repair (Li and Heyer, 2008), the potentially fatal lesion of both backbone strands occurring at a single position along the DNA template caused by a number of internal factors, such as replication fork collapse (Courcelle and Hanawalt, 2003), or external agents, such a free radical attacks on the backbone or irradiative damage. It is therefore crucial for the cell to employ a high fidelity and efficient repair mechanism to prevent loss of chromosome integrity, which could result in mutation or cell death.

The process of HR mediated DNA break damage is depicted in figure 3.1. A single DNA segment is cleaved by a particular damaging agent (Llorente et al., 2008). An exonuclease, such as the RecBCD complex in E.Coli, acts on the free blunt ends of the damaged DNA, removing bases in the 5' to 3' direction, revealing a short segment of single stranded DNA (Singleton et al., 2004; Spies and Kowalczykowski, 2005). The single stranded binding proteins, such as RPA, bind to the newly revealed strand to prevent further damage. This process acts as a precursor to the formation of a ss-DNA filament consisting of RecA in E.Coli or Rad51 in eukaryotes (Galletto et al., 2006; Mazin and Kowalczykowski, 1999; Yang et al., 2005).

Rad51 and RecA act to promote a homology search, in which the complementary DNA sequence from the underlying ssDNA is sought. If the double stranded break occurs during replication fork collapse, the complementary strand would already have been synthesized, and would be in close proximity; likewise, during a meiotic crossover event, the sister chromatids would have aligned previously, and the

homologous region of DNA would be proximal to the Rad51 or RecA filament (Barzel and Kupiec, 2008). The exact details of strand invasion are not currently fully known, but recent structural data from a RecA filament co-crystallized with single stranded DNA indicates that the DNA sequence is exposed in a manner which would promote stable Watson-Crick basepairing of up to six bases exchanged with the intact homologous substrate (Chen et al., 2008).

Once strand exchange has occurred, short segments of the underlying DNA may be filled in by a DNA polymerase, and would complete the heteroduplex structure, while simultaneously disassembling the RecA/Rad51 filament. At this point, the DNA consists of two branch points, known as Holliday junctions, which sit at the crossover regions in the complementary DNA; because of the nearly perfect local sequence homology, the branch points may migrate freely in either direction (Murayama et al., 2008), a process which is expedited by specialized branch migration enzymes (CameriniOtero and Hsieh, 1995). In E.Coli, for instance, the RuvAB motor has been shown to bind the junction and bias its migration over substantial distances (Dawid et al., 2004). The directionality of migration is selected by the binding orientation of the RuvB motor, which is a hexameric ring-shaped helicase that encircles both strands of the DNA (Rasnik et al., 2008). The exact mechanism of binding, and hence selection of a preferred migration orientation, is not known, but may be influenced by the mechanical properties of the junction itself.

The migration of the Holliday junction proceeds until certain recognition sequences, at which point specialized cleavage enzymes, like the E.Coli RuvC resolvase, cut the DNA backbone on opposite strands and resolve the junction (Shah et al., 1997). The result is two fully intact DNA duplexes which may contain varying degrees of

exchanged information, depending on the absolute degree of underlying homology, the direction and extent of branch migration, and the orientation of junction resolution. Homologous recombination events occurring during meiosis can result in gene crossover, which is an important mechanism towards promoting evolutionary diversity (Aylon and Kupiec, 2004). Hence, this well regulated and complicated recombination based pathway provides a high fidelity method by which potentially fatal double stranded DNA lesions may be corrected.

While a large number of the proteins, enzymes, and co-factors which are involved at all points of this pathway have been identified, what is less well understood is the underlying mechanics of the junction migration itself. What are the barriers to effective migration, and what does the energy landscape as the DNA junction point look like? How hard to the motors involved have to push and twist the underlying DNA substrate in order to promote adequate migration? Is it possible that the energetics of the junction itself has an important regulatory function? If such a junction structure can be formed along the DNA, can it serve to reduce torsional buildup, thus reducing the need for the activity of independent enzymes, such as topoisomerases or DNA gyrases? These are the questions our angular optical trapping apparatus is well suited to study.

MATERIALS AND METHODS

The single molecule Holliday junction DNA template was constructed in multiple steps. There were several important parameters which needed to be considered in designing the construct. First, the ends of the molecule needed to be appropriately tagged with multiple linkages for rotationally constrained attachment to the coverslip and the nanofabricated cylinder. Second, the majority of the sequence needed to be fully palindromic to provide a template for fully range of junction branch migration. Finally, a preformed junction with sequence heterology needed to be formed to allow for an easy start to migration when wound in the preferred negative direction, but also providing a heterologous blocking end to prevent total separation of the junction upon positive winding.

To form the construct, two 1.1 kbp palindromic arms were generated via PCR from plasmid pCD1, a modified version of plasmid pRL574. Both arms were amplified from the same sequence with identical lower primers; the upper primer sequences were identical, but in one case the upper primer contained six biotinylated "T" bases and in the other, six digoxygenin "T" bases. The products were then restriction digested with BsaI to generate four bp overhangs with sequence 5'-TTAA.

The preformed Holliday junction with twenty base-pairs of sequence heterology and hairpins at the ends was generated by annealing Hol4 with Hol3-hp and Hol2 with Hol1-hp in annealing buffer (10 mM Tris pH 8.0, 50 mM NaCl, 1 mM EDTA). The single stranded DNA oligos were mixed at equimolar ratios (10 μM final concentration), heated to 94ºC, and slowly cooled to 22ºC over a one hour period.

Sequences of preformed arm segment oligos:

Hol1-hp
5'-TGGTGAAGGAAACTTCACCATTTGATTACGAGATATCGATGCATGCGAATTCGAGCTCC

Hol2
5'-AATTGGAGCTCGAATTCGCATGCATCGATATAATACTTGAGG

Hol3-hp
5'-
GGATCGAAGGAAACTTCGATCCCCTCAAGTATTATATCGATGCATGCGAATTCGAGCTCC

Hol4
5'-AATTGGAGCTCGAATTCGCATGCATCGATATCTCGTAATCAAA

Next, the Hol3hp-4 (Hol1hp-2) products were ligated to the biotin (dig) long palindromic segments at the four bp overhang end for 2 hours at 16ºC. The resulting products consisted of short regions of unpaired bases at the HJ end for further ligation to their complementary segments.

Finally, the Bio-34 and Dig-12 were mixed and ligated for 2 hours at 16ºC, resulting in the construct shown in figure 3.2. The construct is depicted with its junction located at the furthest point along the template; the sequence in the horizontal arms is heterologous, which prevents further travel of the junction along that direction. As shown, negative winding applied to the vertical arms would result in migration of up to 1.1 kbp, the full length of the construct. In practice, this migration would be prohibited upon reaching the biotin and digoxygenin labels near their respective surfaces, just short of the full 1.1 kbp.

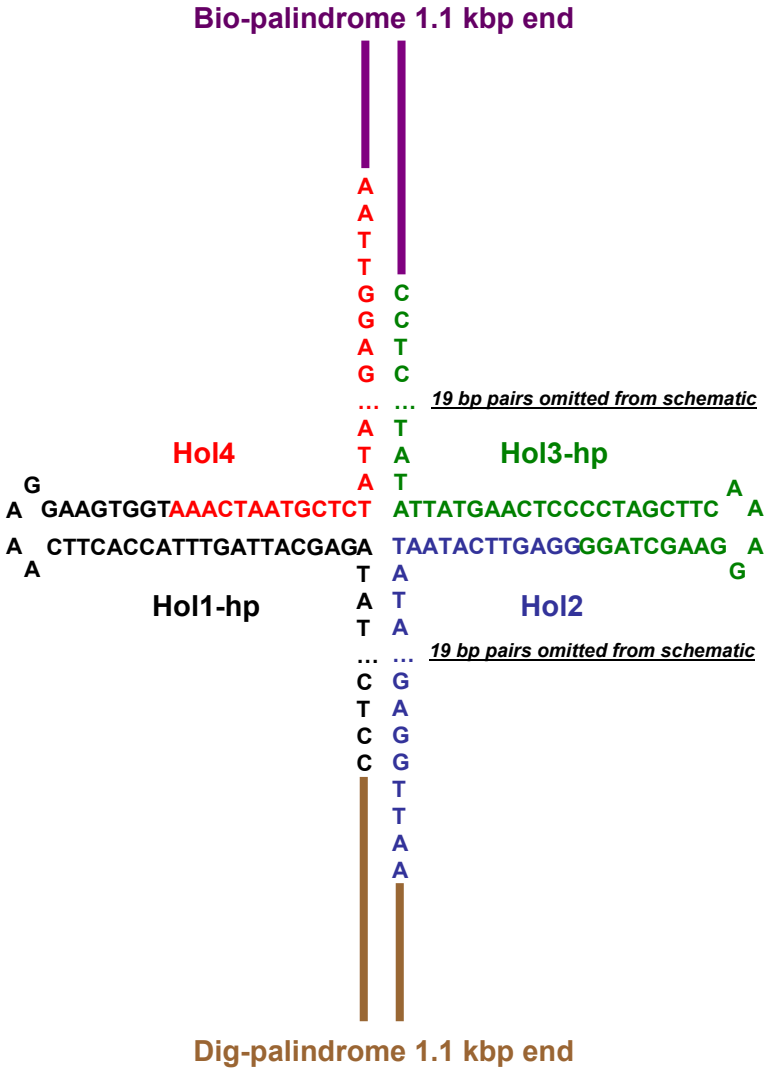

Figure 3.2: Cartoon illustrating the single molecule Holliday junction construct. DNA molecules containing a Holliday junction were created as described in the Materials and Methods section. The preformed arms (Hol1-hp, Hol2, Hol3-hp, and Hol4) contained regions of sequence heterology, which prevented junction migration into the central twenty basepairs of the junction in the arms. This ensured that a Holliday junction in a DNA tether did not collapse prior to measurements and also allowed for easy identification of the end of the migratable palindromic region.

EXPERIMENTAL METHOD

The angular optical trap has been described in detail in previous chapters. In brief, the DNA construct was rotationally constrained at one end to a microscope coverslip and at the other end to a nanofabricated quartz cylinder. The cylinder is trapped in all six lateral and angular dimensions by a linearly polarized optical trap. Twist was added to the molecule by rotation of the cylinder via rotation of the trapping polarization. A constant force was applied along the vertical arms of the junction by monitoring the position of the bead in the trap, and holding it constant via modulation of the position of the coverslip. A cartoon illustrating this experimental configuration is shown as Figure 3.3. To demonstrate that the trap was capable of mechanically migrating the junction over a wide range along the DNA sequence, a tether was held at a constant force (2 pN) and first overwound to form positively supercoiled plectonemic DNA. Negative turns, in the sense of DNA unwinding, were then added over an extensive range (up to -100 turns) to demonstrate that the junction was capable of smoothly migrating over many hundreds of bases (Figure 3.4). In addition, the slope of the extension change during migration per turn added was measured and consistent with the expected extension versus force relation. From this data, the pitch of DNA was found to be 3.65 nm, in good agreement with the crystallographic length of 3.6 nm.

In all subsequent experiments, twenty turns were added to the molecule at a rate of 4 turns/s, first in the sense of DNA unwinding, then immediately in the opposite direction to return the junction back to its original position. The extension data were filtered using a sliding window filter of width 25 ms, while the torque data were filtered with a sliding window of width 2 seconds. All experiments were performed in Phosphate Buffered Saline (pH 7.4), with $[Na^+]$ = 150 mM. A Holliday junction is

known to adopt an "X-stacked" structure in the presence of Mg^{++} ions, preventing junction migration (Panyutin et al., 1995). To eliminate this stacking effect and encourage the active migration of the junction, no Magnesium was used in the experimental buffer.

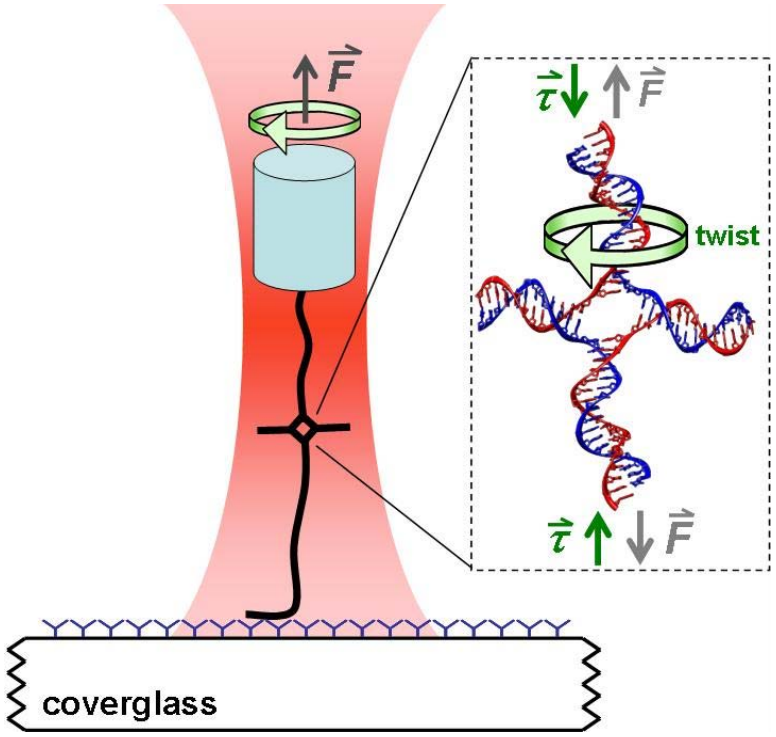

Figure 3.3: Experimental configuration. A single rotationally-constrained DNA tether with a preformed Holliday junction at its center was held in an angular optical trap. Rotation of a trapped quartz cylinder, and hence the end of the DNA molecule attached to it, was performed by rotation of the trapping beam polarization angle. The cartoon inset shows that a Holliday junction is mechanically migrated by the simultaneous application of a tension that opposes arm extrusion and angular constraint at the DNA ends, which gives rise to a torque that encourages the extrusion.

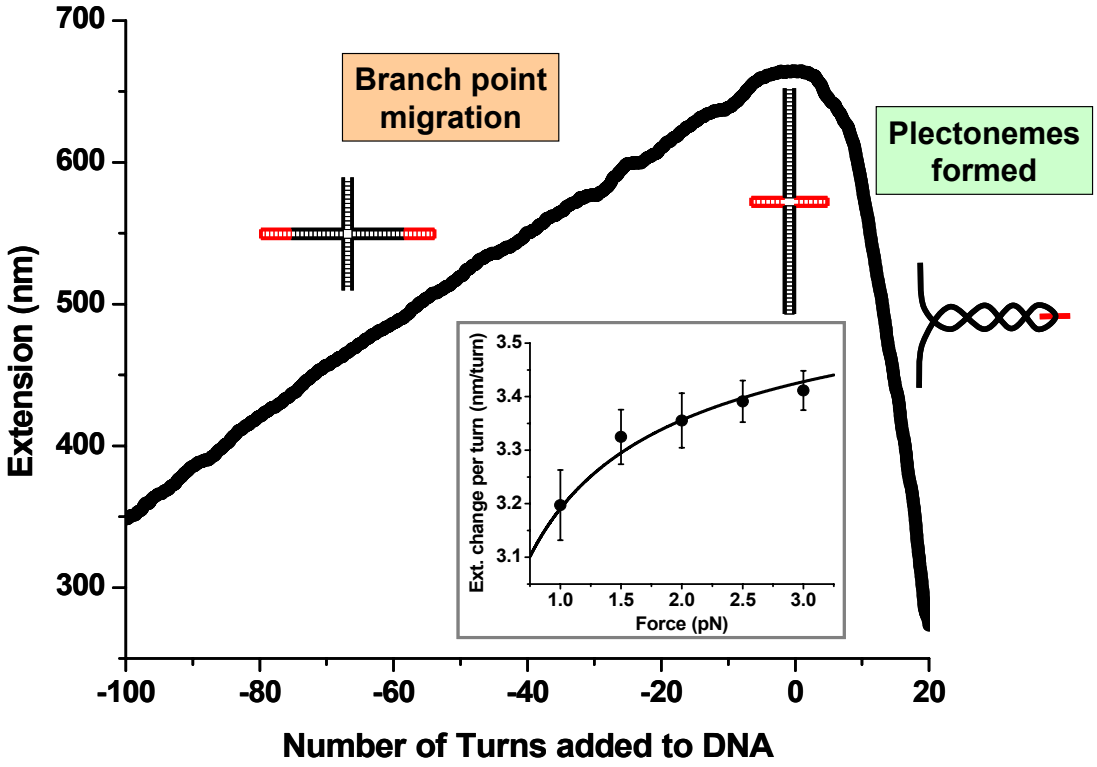

Figure 3.4: Demonstration of Holliday junction migration. A DNA molecule was held at a constant force of 2 pN and overwound, creating positively supercoiled DNA which, after ~8 turns, buckled and formed a plectoneme. The end of the molecule was then rotated in the negative sense up to −100 turns. Below 0 turns, a smooth and continuous migration of the junction was observed over many hundreds of base pairs, as evidenced by a nearly constant rate of decrease in extension. This experiment was repeated at different forces. The inset shows the extension change per turn versus force (black points), which is in excellent agreement with a prediction (black line, DNA pitch = 3.65 nm) from the force-extension relation of dsDNA. This result shows that there was a direct conversion of rotational motion into an extension change, indicating migration of the junction.

RESULTS

During migration, a minute torque, on the order of 1 pN nm, was measured on the DNA in the same sense as DNA underwinding, referred to previously as the 'negative' direction. Multiple molecules were migrated over a twenty turn range at a rate of four turns/second. This process was immediately reversed, and the junction was returned to its original position. The experiment was repeated several times at increasing forces. The results from six individual full experiments were averaged and plotted in figure 3.5. There is a small force dependence on the slope of the extension change, but a clear increase in the absolute value of torque exerted by the junction on the molecule as the tension in the DNA molecule is increased. The measured torque remained constant under a given force but depended strongly on the magnitude of the applied force in a predictable manner.

A similar set of experiments was performed over a wide range of forces (from 1 to 10 pN) on six different DNA molecules. The mean torque measured at each force was pooled, averaged and plotted, as shown in figure 3.6. Error bars shown depict the standard error of the mean.

In addition to the raw data, figure 3.6 shows a theoretical prediction for the dependence of the restoring torque at the junction acting against an applied force. The following section details the derivation of this relationship.

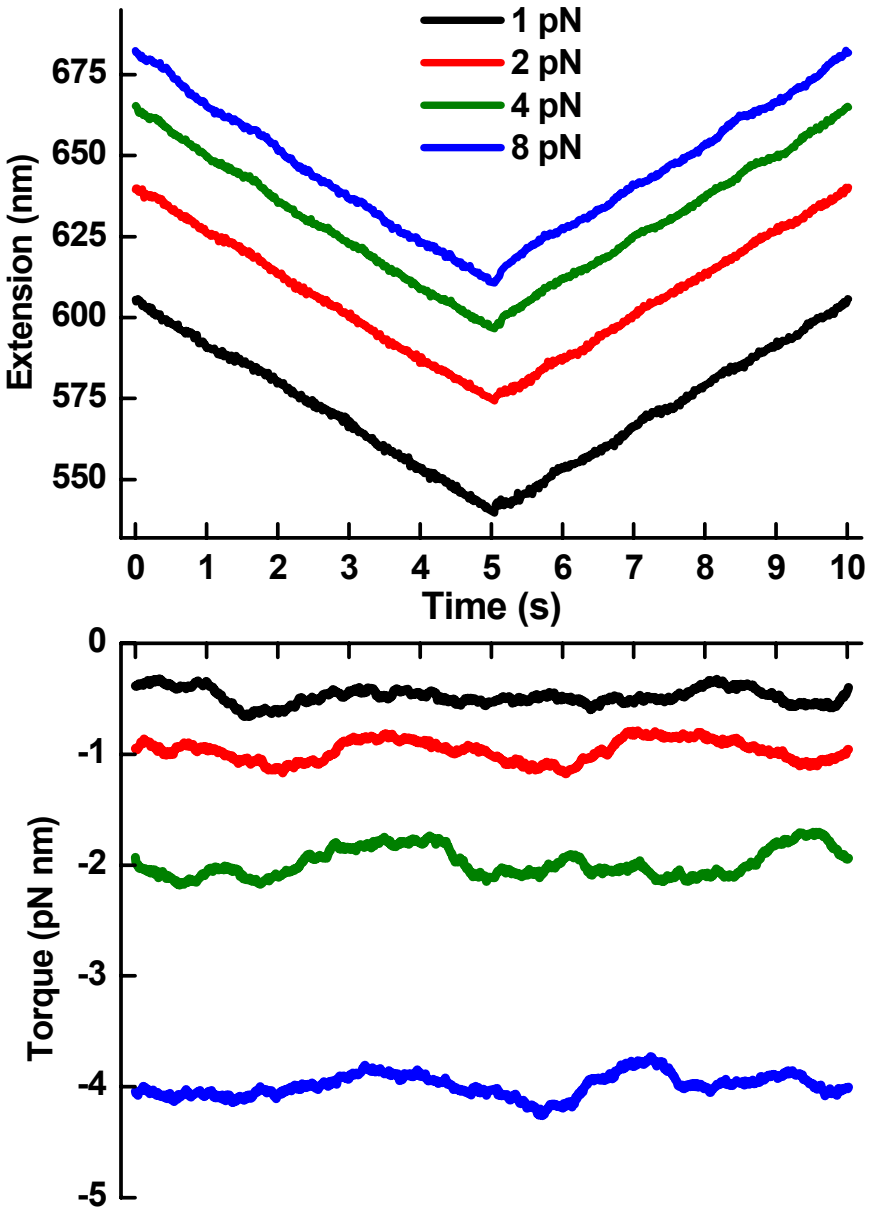

Figure 3.5: Individual extension and torque traces at various applied forces. A single Holliday junction was mechanically migrated over a 20-turn range at 4 turns/s. The migration was then reversed, returning the junction to its original location.

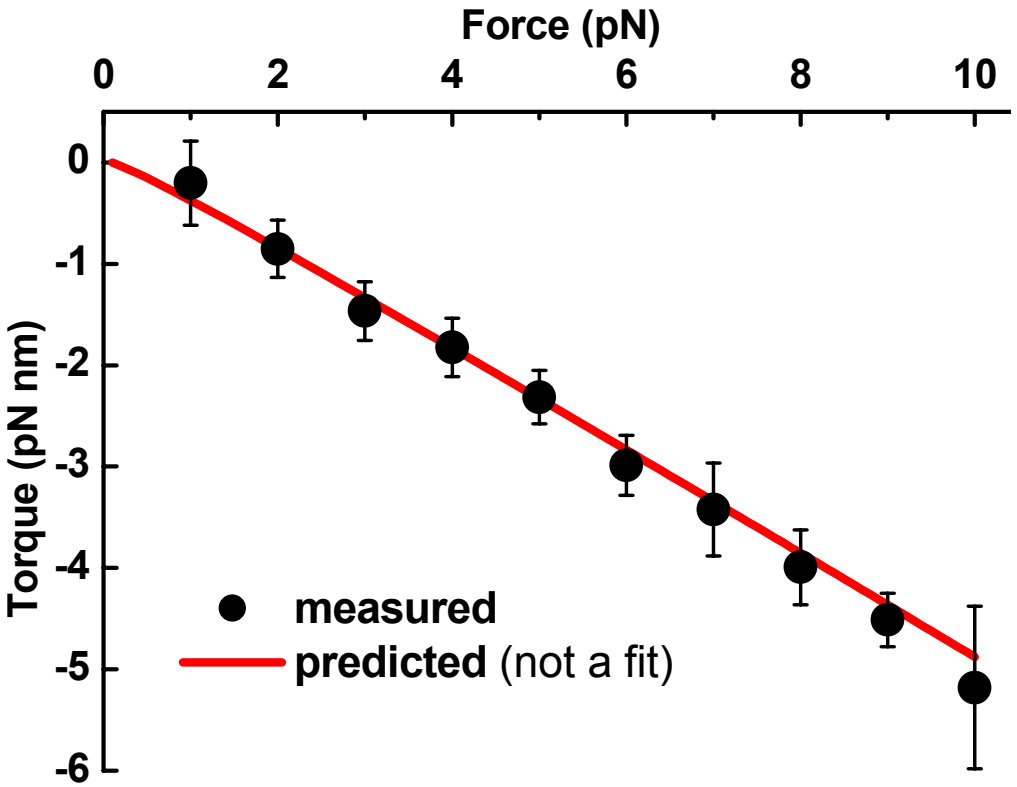

Figure 3.6: The mean torque during migration as a function of force. Shown are the mean torque and its standard deviation (black points, $N = 6$ junctions), as well as a theoretical prediction (red line, not a fit).

DERIVATION OF THE TORQUE-FORCE RELATION OF A HOLLIDAY JUNCTION

An analytical expression for the torque exerted on the DNA based on thermodynamic considerations is derived below.

Consider a DNA molecule containing a Holliday junction which is held under a fixed tension *F* and a fixed angular orientation of one end relative to the other end θ, with a branch point located at base *n* from one end. The free energy for such a system can be written as a sum of a term related to DNA linear elasticity and a term related to DNA torsional elasticity:

$$\Delta G(n;F,\theta) = -2n\int_0^F z_{\mathrm{bp}}(F')dF' + 2n\int_0^{\frac{\theta}{2n}-\frac{2\pi}{10.4}} \tau(\varphi_{\mathrm{bp}})d\varphi_{\mathrm{bp}}$$

where $\tau = \alpha_{\mathrm{bp}}\varphi_{\mathrm{bp}} = \alpha_{\mathrm{bp}}\left(\frac{\theta}{2n} - \frac{2\pi}{10.4}\right)$. α_{bp} is the torsional stiffness for each basepair of dsDNA and φ_{bp} is the angular deviation from the rest angle for each basepair of the dsDNA.

To determine *n* at thermodynamic equilibrium, the free energy is minimized with respect to the branch location *n*:

$$\frac{\partial}{\partial n}\Delta G(n;F,\theta) = 0$$

$$-\int_0^F z_{\mathrm{bp}}(F')dF' + \frac{1}{2}\alpha_{\mathrm{bp}}\left(\frac{\theta}{2n} - \frac{2\pi}{10.4}\right)^2 - \alpha_{\mathrm{bp}}\left(\frac{\theta}{2n} - \frac{2\pi}{10.4}\right)\frac{\theta}{2n} = 0$$

from which the torque τ can be found to be

$$\tau = -\frac{2\pi}{10.4}\alpha_{\mathrm{bp}} + \frac{2\pi}{10.4}\alpha_{\mathrm{bp}}\sqrt{1 - \frac{2\alpha_{\mathrm{bp}}\int_0^F z_{\mathrm{bp}}(F')dF'}{\left(\frac{2\pi}{10.4}\alpha_{\mathrm{bp}}\right)^2}}$$

Over the range of forces used in these experiments, the second term under the square root is <<1. Hence, the torque required to migrate the junction may be simplified as:

$$\tau = -\frac{\alpha_{bp}\int_0^F z_{bp}(F')dF'}{\frac{2\pi}{10.4}\alpha_{bp}} = -\frac{10.4}{2\pi}\int_0^F z_{bp}(F')dF'.$$

Thus, $\tau = -\frac{10.4}{2\pi}\int_0^F z_{\mathrm{bp}}(F')dF'$, where $z_{\mathrm{bp}}(F)$ is the extension versus force relation for a single bp of dsDNA. For higher forces (>1 pN), this may be approximated as, $\tau = -F\frac{\Delta z}{\Delta\theta}$, where Δz is the extension change due to a rotation of $\Delta\theta$ (positive for overwinding). Because one full rotation (2π) should correspond to the migration of one helical pitch of the DNA (approximately 10.4 bp or 3.6 nm), thus $\tau \sim -F\frac{3.6\ \mathrm{nm}}{2\pi}$.

As shown in figure 3.6, the measured torque is in excellent agreement with the thermodynamic prediction.

CONCLUSIONS AND BIOLOGICAL IMPLICATIONS

Based on the measurements presented herein, we propose that the Holliday junction can function as an ultra-sensitive, tunable nano-torque wrench under physiological conditions. The smallest torques measured here are ~ 0.5 pN nm, much smaller than the measured torques required for dsDNA melting (~10 pN nm) (Strick et al., 1999), DNA buckling under similar forces (~ 20 pN nm) (Forth et al., 2008), and phase transitions to P- and supercoiled P-forms of DNA (> 35 pN nm) (Bryant et al., 2003). During recombination or dsDNA break repair events, the migrating Holliday junction could act as a torque buffer and prevent the formation of torsionally generated DNA structures, such as plectonemes or melted DNA bubbles. Cruciform extrusion at the sites of inverted repeat sequences is also known to have a regulatory function, and may similarly serve to alleviate torsional stress in nearby DNA. While topological structures can be alleviated via the action of topoisomerases or DNA gyrases, torsional relaxation via migration would reduce the need for such activity and could greatly assist the progression of junction bound motors, allowing for efficient coupling of rotation to translocation and torque to force.

REFERENCES

Aylon, Y., and Kupiec, M. (2004). New insights into the mechanism of homologous recombination in yeast. Mutat Res-Rev Mutat Res *566*, 231-248.

Barzel, A., and Kupiec, M. (2008). Finding a match: how do homologous sequences get together for recombination? Nat Rev Genet *9*, 27-37.

Bryant, Z., Stone, M.D., Gore, J., Smith, S.B., Cozzarelli, N.R., and Bustamante, C. (2003). Structural transitions and elasticity from torque measurements on DNA. Nature *424*, 338-341.

CameriniOtero, R.D., and Hsieh, P. (1995). Homologous recombination proteins in prokaryotes and eukaryotes. Annu Rev Genet *29*, 509-552.

Chen, Z.C., Yang, H.J., and Pavletich, N.P. (2008). Mechanism of homologous recombination from the RecA-ssDNA/dsDNA structures. Nature *453*, 489-U483.

Courcelle, J., and Hanawalt, P.C. (2003). RecA-dependent recovery of arrested DNA replication forks. Annu Rev Genet *37*, 611-646.

Dawid, A., Croquette, V., Grigoriev, M., and Heslot, F. (2004). Single-molecule study of RuvAB-mediated Holliday-junction migration. Proc Natl Acad Sci U S A *101*, 11611-11616.

Dawid, A., Guillemot, F., Breme, C., Croquette, V., and Heslot, F. (2006). Mechanically controlled DNA extrusion from a palindromic sequence by single molecule micromanipulation. Physical Review Letters *96*, 188102.

Deufel, C., Forth, S., Simmons, C.R., Dejgosha, S., and Wang, M.D. (2007). Nanofabricated quartz cylinders for angular trapping: DNA supercoiling torque detection. Nat Methods *4*, 223-225.

Forth, S., Deufel, C., Sheinin, M.Y., Daniels, B., Sethna, J.P., and Wang, M.D. (2008). Abrupt buckling transition observed during the plectoneme formation of individual DNA molecules. Physical Review Letters *100*, 148301.

Galletto, R., Amitani, I., Baskin, R.J., and Kowalczykowski, S.C. (2006). Direct observation of individual RecA filaments assembling on single DNA molecules. Nature *443*, 875-878.

Kowalczykowski, S.C., Dixon, D.A., Eggleston, A.K., Lauder, S.D., and Rehrauer, W.M. (1994). Biochemistry Of Homologous Recombination in Escherichia-Coli. Microbiol Rev *58*, 401-465.

La Porta, A., and Wang, M.D. (2004). Optical torque wrench: Angular trapping, rotation, and torque detection of quartz microparticles. Physical Review Letters *92*, 190801.

Li, X., and Heyer, W.D. (2008). Homologous recombination in DNA repair and DNA damage tolerance. Cell Res *18*, 99-113.

Llorente, B., Smith, C.E., and Symington, L.S. (2008). Break-induced replication - What is it and what is it for? Cell Cycle *7*, 859-864.

Mazin, A.V., and Kowalczykowski, S.C. (1999). A novel property of the RecA nucleoprotein filament: activation of double-stranded DNA for strand exchange in trans. Genes Dev *13*, 2005-2016.

Murayama, Y., Kurokawa, Y., Mayanagi, K., and Iwasaki, H. (2008). Formation and branch migration of Holliday junctions mediated by eukaryotic recombinases. Nature *451*, 1018-U1010.

Panyutin, I.G., Biswas, I., and Hsieh, P. (1995). A Pivotal Role for the Structure of the Holliday Junction in DNA Branch Migration. Embo J *14*, 1819-1826.

Panyutin, I.G., and Hsieh, P. (1994). The Kinetics of Spontaneous DNA Branch Migration. Proc Natl Acad Sci U S A *91*, 2021-2025.

Pearson, C.E., Zorbas, H., Price, G.B., and ZannisHadjopoulos, M. (1996). Inverted repeats, stem-loops, and cruciforms: Significance for initiation of DNA replication. J Cell Biochem *63*, 1-22.

Rasnik, I., Jeong, Y.J., McKinney, S.A., Rajagopal, V., Patel, S.S., and Ha, T. (2008). Branch migration enzyme as a Brownian ratchet. Embo J *27*, 1727-1735.

Shah, R., Cosstick, R., and West, S.C. (1997). The RuvC protein dimer resolves Holliday junctions by a dual incision mechanism that involves base-specific contacts. Embo J *16*, 1464-1472.

Singleton, M.R., Dillingham, M.S., Gaudier, M., Kowalczykowski, S.C., and Wigley, D.B. (2004). Crystal structure of RecBCD enzyme reveals a machine for processing DNA breaks. Nature *432*, 187-193.

Spies, M., and Kowalczykowski, S.C. (2005). Homologous recombination by the RecBCD and RecF pathways (Amer Soc Microbiology).

Strick, T.R., Bensimon, D., and Croquette, V. (1999). Micro-mechanical measurement of the torsional modulus of DNA. Genetica *106*, 57-62.

van Gent, D.C., Hoeijmakers, J.H.J., and Kanaar, R. (2001). Chromosomal stability and the DNA double-stranded break connection. Nat Rev Genet *2*, 196-206.

Yang, H.J., Li, Q.B., Fan, J., Holloman, W.K., and Pavletich, N.P. (2005). The BRCA2 homologue Brh2 nucleates RAD51 filament formation at a dsDNA-ssDNA junction. Nature *433*, 653-657.